IOPscience iopscience.iop.org

Home Search Collections Journals About Contact us My IOPscience

A posteriori error estimates in a globally convergent FEM for a hyperbolic coefficient inverse problem

This article has been downloaded from IOPscience. Please scroll down to see the full text article.

2010 Inverse Problems 26 115007

(http://iopscience.iop.org/0266-5611/26/11/115007)

View the table of contents for this issue, or go to the journal homepage for more

Download details:
IP Address: 129.16.126.212
The article was downloaded on 07/10/2010 at 15:51

Please note that terms and conditions apply.

Inverse Problems **26** (2010) 115007 (34pp) doi:10.1088/0266-5611/26/11/115007

A posteriori error estimates in a globally convergent FEM for a hyperbolic coefficient inverse problem

M Asadzadeh and L Beilina[1]

Department of Mathematics, Chalmers University of Technology and Gothenburg University, SE-412 96 Goteborg, Sweden

E-mail: mohammad@chalmers.se and larisa.beilina@chalmers.se

Received 29 March 2010, in final form 17 July 2010
Published 30 September 2010
Online at stacks.iop.org/IP/26/115007

Abstract

This study concerns *a posteriori* error estimates in a globally convergent numerical method for a hyperbolic coefficient inverse problem. Using the Laplace transform the model problem is reduced to a nonlinear elliptic equation with a gradient dependent nonlinearity. We investigate the behavior of the nonlinear term in both *a priori* and *a posteriori* settings and derive optimal *a posteriori* error estimates for a finite-element approximation of this problem. Numerical experiments justify the efficiency of *a posteriori* estimates in the globally convergent approach.

(Some figures in this article are in colour only in the electronic version)

1. Introduction

This paper is a further development of studies in [1–3] and [16] where a new globally convergent approximation method was proposed and numerically tested. In a recent publication [14] this method was verified on blind imaging of the experimental data measured in picoseconds' scale regime. Application areas of inverse algorithms range from detection of explosives in airport security to medical optical imaging, etc.

Compared with [1–3, 14, 16] the main new element of this work is that we perform an adaptive finite-element technique directly inside the globally convergent method. We focus on the derivation of optimal *a posteriori* error estimates for a finite-element approximation of a nonlinear elliptic integro-differential equation, formulate a new globally convergent adaptive algorithm and apply it in the numerical study for the model problem in two dimensions.

A numerical method is called *globally convergent* if (i) a rigorous convergence analysis is available, independent of the quality of an initial guess for the exact solution and (ii) the convergence properties are justified by numerical simulations. Generally, a *locally convergent*

[1] Author to whom any correspondence should be addressed.

 © 2010 IOP Publishing Ltd Printed in the UK & the USA

numerical method may yield a *global* exact solution only if the initial guess lies in a small neighborhood of the exact solution. A direct numerical approach to solve a coefficient inverse problem (CIP) is a minimization procedure for the least-squares residual functional. This, however, suffers from the drawback of the presence of multiple local minima for the functionals. To circumvent such an obstacle in [12] a new convexification algorithm was developed for the solution of one-dimensional CIP in the imaging of dielectric permittivity of media. This algorithm was later extended in [15] to the multidimensional case with applications to diffusive optical mammography. The convexification algorithm belongs to the first generation of globally convergent numerical methods. Further developments of globally convergent algorithms were started in [1–3], where the layer-stripping procedure was performed with respect to the pseudo-frequency rather than the spatial variable which is the case in the convexification. Also, the Carleman weight function in [1–3] depends on the pseudo-frequency rather than on the spatial variable, as in the works [12, 15]. These new components contribute to a better stability in the globally convergent reconstruction algorithm.

There are also some other numerical methods for multidimensional CIPs, which do not use a good first guess for the solution. The methods described in [19, 20] and [18] were developed for CIPs for some elliptic equations with fixed frequency, and their numerical implementations in 2D can be found respectively in [8] and [17]. The method described in [5] was developed for CIPs for some hyperbolic equations. Numerical implementation in [5] can be found in [6]. Unlike the current paper, they work for some CIPs with the data resulting from multiple measurements, i.e. either with many positions of the point source or many directions of the initializing plane wave.

An alternative approach to solve CIP is a synthesis of a globally convergent numerical method and a strongly converging (local) scheme such as the adaptive finite-element procedure. In [2, 3] it was shown that the globally convergent numerical method provides a good initial guess for the locally convergent adaptive finite-element method. A first application of these results for the acoustic wave equation shows a good performance [2, 3]. Compared to [2, 3], this work concerns a new such combination, where the adaptivity procedure is performed directly inside the globally convergent algorithm. For this scheme we develop *a posteriori* error estimates and prove convergence rates justifying the accuracy of the method.

Compared with [2, 3] a new combination of the adaptivity technique inside the globally convergent method allows us to reconstruct shape, contrast and location of inclusions more accurately and faster. In [2, 3] we apply the adaptivity technique after a globally convergent method. The main idea of [2, 3] is that we used the two-stage numerical procedure to reconstruct the unknown coefficient: in the first stage we obtain the solution in a globally convergent method, and in the second stage, this approximation is taken as the starting point for the adaptivity technique, which provides an enhancement, i.e. a better approximation for the correct solution. The adaptivity technique is then performed on minimization of the least-squares objective functional on a sequence of locally adaptively refined meshes in a series of steps until images are stabilized. Compared with [2, 3] the new method proposed in this paper has two main advantages: (i) it is faster, since instead of solving time-dependent forward and adjoint problems in space and time on every mesh in the adaptivity technique of [2, 3], in the current adaptive version of the globally convergent algorithm we solve the elliptic nonlinear integro-differential equation only in space; (ii) more efficient, since we perform the adaptivity technique directly inside the globally convergent method and thus, we develop the adaptive globally convergent algorithm instead of using the two-stage numerical procedure. We also note that the proposed method has similar results of reconstruction as the two-stage numerical procedure of [2, 3], see also the remark in section 8.

The new element of this paper is that we numerically test the new method on the reconstruction of the medium with the varying function $c(x)$ compared with the reconstruction of small inclusions of previous works [2, 3]. Our numerical results show that the adaptive globally convergent algorithm can image only the maximal contrast of the reconstructed function compared to the background medium. Nevertheless, this is obvious in the practical applications, when only maximal values of the media should be known.

An outline of this paper is as follows: in section 2 we formulate both forward and inverse problems and transfer the inverse problem to a Dirichlet boundary value problem for a nonlinear integro-differential equation where the unknown coefficient is removed. In section 3 we formulate the layer-stripping procedure with respect to $s > 0$, the parameter of the Laplace transform in the original hyperbolic PDE. Note that we do not use the inverse Laplace transform, since approximations for the unknown coefficient are obtained in the 'Laplace domain'. In section 4 we introduce a finite-element method, derive bounds for coefficients and formulate a dual problem. Section 5 is devoted to the derivation of bounds for the nonlinear operator and *a priori* error estimates. In section 6 we develop reliable and efficient *a posteriori* error estimates for the full problem. In section 7 we present a new adaptive globally convergent algorithm based on the *a posteriori* error estimate of section 6. Finally, in section 8 we present the results of reconstruction of the function in two dimensions using the adaptive globally convergent algorithm.

2. Preliminaries: statements of forward and inverse problems

Consider the Cauchy problem for the hyperbolic equation

$$c(x)u_{tt} = \Delta u \qquad \text{in} \quad \mathbb{R}^3 \times (0, \infty), \tag{2.1}$$

$$u(x, 0) = 0, \qquad u_t(x, 0) = \delta(x - x_0). \tag{2.2}$$

Equation (2.1) governs a wide range of application areas. The combination (2.1) and (2.2) describes, e.g., the propagation of acoustic and electromagnetic waves. See [9] for a derivation of (2.1) from Maxwell's equation in the 2D case. We shall assume that $c(x)$ satisfies the following conditions: given positive constants d_1 and d_2, $d_1 < d_2$:

$$\begin{aligned} &c(x) \in C^2(\mathbb{R}^3), \qquad 2d_1 \leqslant c(x) \leqslant 2d_2 \\ &\text{and} \qquad c(x) = 2d_1 \qquad \text{for} \quad x \in \mathbb{R}^3 \setminus \Omega, \qquad \Omega \subset \mathbb{R}^3. \end{aligned} \tag{2.3}$$

A priori knowledge of constants d_1, d_2 corresponds well with the Tikhonov concept for ill-posed problems [30]. In applications the assumption $c(x) = 2d_1$ for $x \in \mathbb{R}^3 \setminus \Omega$ means that the target coefficient $c(x)$ has a known constant value outside of the medium of interest Ω. Another argument here is that one should bound the coefficient $c(x)$ from the below by a positive number to ensure that the operator in (2.1) is a hyperbolic one on all iterations of our method. Since we do not impose any 'smallness' conditions on numbers d_1 and d_2, smallness conditions are also not imposed on the unknown coefficient. Hence, a numerical method developed in [3] is a globally convergent one.

We determine $c(x)$ for $x \in \Omega$ assuming that the boundary data, $g(x, t)$ below, is known for a point source acting at $x_0 \notin \overline{\Omega}$:

$$u(x, t) = g(x, t), \qquad \forall (x, t) \in \partial\Omega \times (0, \infty). \tag{2.4}$$

The function $g(x, t)$ models time-dependent measurements of the wave field at the boundary of the domain where the coefficient should be reconstructed. In the case of a finite time interval, on which measurements are performed, one should assume that this interval is quite

large and thus, the t-integral of the Laplace transform over this interval is approximately the same as the one over $(0, \infty)$. The uniqueness theorem for this inverse problem is a long standing and well-known open question. This question is addressed positively via Carleman estimates only in the case when the δ-function in (2.2) is replaced with a function which is nonvanishing in the entire domain $\overline{\Omega}$ [16, 17]. By our opinion we assume that the uniqueness for our CIP holds because of applications, see also [18].

Now, we use the Laplace transform

$$w(x,s) = \int_0^\infty u(x,t)\,\mathrm{e}^{-st}\,\mathrm{d}t \qquad \text{for} \quad s > \underline{s} > 0, \tag{2.5}$$

where $\underline{s}$ is a constant called *the pseudo-frequency*. Recall that it suffices to choose $\underline{s}$ such that the integral (2.5) and its first partial derivatives in x and t converge. Then w satisfies the equation

$$\Delta w - s^2 c(x) w = -\delta(x - x_0)c(x_0), \qquad \forall\, s \geqslant \underline{s} > 0, \tag{2.6}$$

with the following condition at infinity:

$$\lim_{|x|\to\infty} w(x,s) = 0, \qquad \forall\, s \geqslant \underline{s} > 0. \tag{2.7}$$

In [3] it was proven that the limit in (2.7) is positive.

2.1. *The nonlinear integro-differential equation with the eliminated unknown coefficient*

Since it was established in [3] that $w(x,s) > 0$, we can consider the function $v(x,s) = \ln w$, since $x_0 \notin \overline{\Omega}$, and then (2.6) and (2.7) yield

$$\Delta v + |\nabla v|^2 = s^2 c\,(x) \quad \text{in } \Omega, \tag{2.8}$$

$$v\,(x,s) = \ln \varphi\,(x,s)\,, \qquad \forall\,(x,s) \in \partial\Omega \times [\underline{s}, \overline{s}], \tag{2.9}$$

where $\varphi\,(x,s)$ is the Laplace transform of the data function $g\,(x,t)$. We eliminate the coefficient $c\,(x)$ by differentiating (2.8) with respect to s. To single out the unknown coefficient $c\,(x)$ in (2.8), we introduce a new function

$$H(x,s) = \frac{v}{s^2}. \tag{2.10}$$

Further, assuming certain regularity conditions (see, e.g., [1]), it follows from (2.10) that, for $|\alpha| \leqslant 2$,

$$D_x^\alpha(H) = O\left(\frac{1}{s}\right), \qquad D_x^\alpha D_s(H) = O\left(\frac{1}{s^2}\right), \qquad s \to \infty. \tag{2.11}$$

By (2.8) and (2.10), H satisfies

$$\Delta H + s^2\,|\nabla H|^2 = c\,(x)\,. \tag{2.12}$$

Next we let

$$q\,(x,s) = \partial_s H\,(x,s)\,; \tag{2.13}$$

then, by (2.11) and (2.13)

$$H\,(x,s) = -\int_s^\infty q\,(x,\tau)\,\mathrm{d}\tau := -\int_s^{\overline{s}} q\,(x,\tau)\,\mathrm{d}\tau + V\,(x,\overline{s})\,, \tag{2.14}$$

where $\overline{s} > s_0$ is a large number and

$$V\,(x,\overline{s}) = H\,(x,\overline{s}) = \frac{\ln w\,(x,\overline{s})}{\overline{s}^2}. \tag{2.15}$$

The unknown function $V(x, \overline{s})$ is called the *tail function*. To determine V we need the parameter $\overline{s}$ which we choose numerically. Therefore, (2.15) is an approximation rather than an equality. By (2.11) and (2.15) the tail is small for large values of $\overline{s}$. Usually, the tail function is put to zero. Here we include V either on the right-hand side in iteration steps as a data or study it as an unknown in a coupled system of equations.

Now differentiating (2.12) with respect to s, from (2.14)–(2.15) we obtain the following nonlinear integro-differential equation for $q = q(x, s)$:

$$\Delta q - 2s^2 \nabla q \cdot \int_s^{\overline{s}} \nabla q(x, \tau)\, \mathrm{d}\tau + 2s \left[\int_s^{\overline{s}} \nabla q(x, \tau)\, \mathrm{d}\tau \right]^2 + 2s^2 \nabla q \nabla V - 2s \nabla V \cdot \int_s^{\overline{s}} \nabla q(x, \tau)\, \mathrm{d}\tau + 2s (\nabla V)^2 = 0. \tag{2.16}$$

Further, by (2.9), (2.10) and (2.13) we may impose the following Dirichlet boundary condition:

$$q(x, s) = \psi(x, s), \qquad \forall (x, s) \in \partial\Omega \times [\underline{s}, \overline{s}], \tag{2.17}$$

where ψ satisfies

$$\psi(x, s) = \frac{\varphi_s}{\varphi s^2} - \frac{2 \ln \varphi}{s^3}.$$

Suppose that q and its partial derivatives of order up to 2 in x: $D_x^\alpha q$, $|\alpha| \leqslant 2$ are already approximated. Then, the coefficient $c(x)$ can be, approximately, determined using (2.12):

$$c(x) = \Delta H + \underline{s}^2 (\nabla H)^2, \tag{2.18}$$

where H is given by (2.14), which requires an initial guess for V as well. In the absence of integral terms and if the tail function were known, (2.16) would be the classical Dirichlet boundary value problem for the Laplace equation. However, the presence of the integral term, because of its nonlinearity, is the main source of complexity. Another difficulty is the presence of two unknowns, q and V, in equation (2.16). We may overcome this difficulty by treating q and V differently: while we iteratively find approximations for q 'restricted' only to equation (2.16), we determine updates for V using solutions for (2.1), (2.2) and relation (2.15).

3. A sequence of elliptic Dirichlet boundary value problems

In this section we approximate $q(x, s)$ with a piecewise constant function with respect to the pseudo-frequency s. Assume that there exists a partition $\underline{s} = s_N < s_{N-1} < \cdots < s_1 < s_0 = \overline{s}$, $s_{n-1} - s_n = k$ of the interval $[\underline{s}, \overline{s}]$ with a sufficiently small and uniform step size k such that $q(x, s) = q_n(x)$ for $s \in (s_n, s_{n-1})$. Hence,

$$\int_s^{\overline{s}} \nabla q(x, \tau)\, \mathrm{d}\tau = (s_{n-1} - s) \nabla q_n(x) + k \sum_{j=1}^{n-1} \nabla q_j(x), \qquad s \in (s_n, s_{n-1}). \tag{3.1}$$

We also approximate the boundary condition (2.17) as a piecewise constant function on s:

$$q_n(x) = \overline{q}_n(x), \qquad x \in \partial\Omega, \qquad j = 1, \ldots, n, \tag{3.2}$$

where

$$\overline{q}_n(x) = \frac{1}{k} \int_{s_n}^{s_{n-1}} q(x, s)\, \mathrm{d}s. \tag{3.3}$$

On each subinterval $(s_n, s_{n-1}]$, $n \geqslant 1$, we assume that the functions $q_j(x)$, $j = 1, \ldots, n-1$, are known. In this way, for each n, $n = 1, \ldots, N$, we obtain an approximate equation for

$q_n(x)$. Now we insert (3.1) in (2.16) and multiply the resulting equation by the Carleman weight function (CWF)

$$C_{n,\lambda}(s) = \mathrm{e}^{\lambda(s-s_{n-1})}, \qquad s \in (s_n, s_{n-1}], \qquad \lambda \gg 1, \tag{3.4}$$

and integrate over $s \in (s_n, s_{n-1}]$. (To choose λ see theorem 6.1 in [1].) We obtain for $n = 1, \ldots, N$

$$\begin{aligned}\tilde{\mathcal{L}}_{n,\varepsilon}(q_n, V_n) &:= \mathcal{L}_n(q_n, V_n) - \varepsilon q_n := \Delta q_n - A_{1,n}\left(k\sum_{i=1}^{n-1}\nabla q_i\right)\nabla q_n + A_{1n}\nabla q_n \nabla V_n - \varepsilon q_n \\ &\approx 2\frac{I_{1,n}}{I_0}(\nabla q_n)^2 - A_{2,n}k^2\left(\sum_{i=1}^{n-1}\nabla q_i(x)\right)^2 \\ &\quad + 2A_{2,n}\nabla V_n\left(k\sum_{i=1}^{n-1}\nabla q_i\right) - A_{2,n}(\nabla V_n)^2. \end{aligned} \tag{3.5}$$

The term $-\varepsilon q_n$ is added for regularizing purpose. It is straightforward to compute the coefficients

$$\begin{aligned} I_0 &:= I_0(\lambda, k) = \int_{s_n}^{s_{n-1}} C_{n,\lambda}(s)\,\mathrm{d}s, \\ I_{1,n} &:= I_{1,n}(\lambda, k) = \int_{s_n}^{s_{n-1}} s(s_{n-1}-s)[s-(s_{n-1}-s)]C_{n,\lambda}(s)\,\mathrm{d}s, \\ A_{1,n} &:= A_{1,n}(\lambda, k) = \frac{2}{I_0}\int_{s_n}^{s_{n-1}} s[s-2(s_{n-1}-s)]C_{n,\lambda}(s)\,\mathrm{d}s, \\ A_{2,n} &:= A_{2,n}(\lambda, k) = \frac{2}{I_0}\int_{s_n}^{s_{n-1}} sC_{n,\lambda}(s)\,\mathrm{d}s. \end{aligned}$$

Then we have obtained the Dirichlet boundary value problem (3.5), with the boundary condition (3.2), for a nonlinear elliptic PDE with the unknown function $q_n(x)$, $n = 1, \ldots, N$. In this system the tail function V is also unknown. An important observation is that

$$\frac{|I_{1,n}(\lambda, k)|}{I_0(\lambda, k)} \leqslant \frac{4\bar{s}^2}{\lambda} \quad \text{for } \min(\lambda k, \bar{s}) \geqslant 1. \tag{3.6}$$

Therefore, taking $\lambda \gg 1$ we mitigate the influence of the nonlinear term with $(\nabla q_n)^2$ in (3.5), which enables us to solve a linear problem on each iterative step. Further, with λ and $\bar{s}$ as in (3.6)

$$\max_{1\leqslant n\leqslant N}\{|A_{1,n}| + |A_{2,n}|\} \leqslant 8\bar{s}^2. \tag{3.7}$$

3.1. Global convergence

To study equation (3.5) and prove the *a posteriori* error estimate for the function q_n of that equation we shall need bounds of the coefficients in a modified version of (3.5) and the corresponding error equation. All bounds in lemma 3.1 follows from definitions of different constants and proof of theorem 6.1 of [3], see section 6. Now, for convenience of readers, we briefly recall some definitions given in [3] which are used in lemmas 3.1 and 4.1.

Let $c^\star$, $q^\star$ and $V^\star$ be the exact solutions corresponding to the approximations c_n, q_n and V_n, respectively. We also use the positive constant $M^* = M^*(\|q^*\|_{C^{2+\alpha}(\overline{\Omega})\times C^1[\underline{s},\bar{s}]}, \bar{s}) = M^*(C^*, \bar{s})$, $0 < \alpha < 1$, and then

$$M^* = 2C^* \max\left(8\bar{s}^2, \max_{1\leqslant n\leqslant N}\left\{\left|A_{1,n}\right| + \left|A_{2,n}\right|\right\}\right) = 16C^*\bar{s}^2, \qquad C^* \geqslant 1. \tag{3.8}$$

For any function $c(x) \in C^{\alpha}(\mathbb{R}^3)$ such that $c(x) \geqslant d_1$, $c(x) = 2d_1$ for $x \in R^3 \setminus \Omega$ consider the solution $w_c(x, \overline{s}) \in C^3(\mathbb{R}^3 \setminus \{|x - x_0| < r\}), \forall r > 0$ of the problem (2.6), (2.7) and let $V_c(x) = (\overline{s})^{-2} \ln w_c(x, \overline{s}) \in C^{2+\alpha}(\overline{\Omega})$ be the corresponding tail function. Assume that

$$\max(|V^*|_{2+\alpha}, |V_c|_{2+\alpha}, |V_{1,1}|_{2+\alpha}) \leqslant \xi \qquad \text{and} \qquad \|\bar{\psi}^{\star}{}_n - \bar{\psi}_n\|_{C^{2+\alpha}(\partial\Omega)} \leqslant C^{\star}(k + \sigma), \quad (3.9)$$

where $\xi \in (0, 1)$ and $\sigma \in (0, 1)$ are sufficiently small numbers. Here, σ characterizes the level of the error in data $\psi(x, s)$. Let $V_{1,1}(x, \overline{s}) \in C^{2+\alpha}(\overline{\Omega})$ be the initial tail. Further, let $\eta := 2(k + \sigma + \xi + \varepsilon)$ and $\overline{N} \leqslant N$ (where N is the total number of functions q_n calculated by the algorithm) be related to the step size k by $\overline{N}(k)\, k = \beta \leqslant \frac{1}{24KM^*}$. Here, ε is the regularization parameter for equation (3.5) and $K > 0$ is a constant in the Shauder theorem, see (6.17) in [3] for details. Finally, we assume that

$$\eta \leqslant \eta_0 = \min \frac{1}{8}\left(\frac{1}{2KM^{\star}}, 3d_1\right), \qquad \lambda \geqslant \lambda_0 = \max\left(\frac{(C^*)^2}{4}, 3KM^*, \frac{1}{\eta^2}\right), \quad (3.10)$$

where η_0 and λ_0 are initial parameter values. Now, with q_n^* denoting a first-order approximation of q^* in $(s_n, s_{n-1}]$ we can prove the following convergence lemma (follows from theorem 6.1 [3]).

Lemma 3.1. *Assume that all conditions of theorem 6.1 [3], conditions (3.9) and (3.10) hold; then, for each $n \in [1, \bar{N}]$ the following estimates take place*

$$|q_n - q_n^*|_{2+\alpha} \leqslant 2KM^*\left(\frac{1}{\sqrt{\lambda}} + 3\eta\right), \qquad n \in [1, \overline{N}], \quad (3.11)$$

$$|q_n|_{2+\alpha} \leqslant 2M^*, \qquad n \in [1, \overline{N}], \quad (3.12)$$

$$|c_n - c^*|_{\alpha} \leqslant \frac{\eta}{2 \cdot 9^{n-1}} + \frac{23}{8}\eta, \qquad n \in [2, \overline{N}]. \quad (3.13)$$

Remark 1. In [3] the proof of the globally convergent theorem is based on the Shauder theorem which uses *Hölder* norms. Our estimates above are based on the proof of theorem 6.1 of [3] and thus also use *Hölder* norms. Since practically we are working in finite-dimensional spaces where all norms are equivalent we can replace *Hölder* norms to more convenient for computations L^2 norms, what we do in the derivation of *a posteriori* error estimation below.

4. A finite-element discretization

We approximate the solution for (3.5) by a finite-element method with continuous piecewise linear basis functions on *a partially structured mesh* in space and implement the resulting scheme using a hybrid code similar to the one developed in [4]. More specifically, we decompose the computational spatial domain G into $\Omega \subset G$ (typically, covering only a small part of G) and $\Omega^c = G \setminus \Omega$, and discretize Ω by an unstructured mesh and Ω^c by a quasi-uniform mesh. To discretize Ω^c we use quadrilateral elements in 2D and hexahedra in the 3D case. In Ω, for each n, we use a partition $\mathcal{T}_{n,h} = \{K\}$ with elements K. We associate with $\mathcal{T}_{n,h}$ a piecewise continuous mesh function $h = h(x)$ representing the diameter of the element K containing x. We use the L_2-inner product and norm

$$(u, v) = \int_{\Omega} uv \, \mathrm{d}x, \qquad \|u\|^2 = (u, u).$$

Choosing $c(x) = 1$ for $x \in \Omega^c$, and then given $g(x, t) = u|_{\partial\Omega}$, we can uniquely determine the function $u(x, t)$ for $(x, t) \in (\Omega^c) \times (0, T)$ as the solution of the boundary value problem

for equation (2.1) with boundary conditions on both boundaries ∂G and $\partial\Omega$. Hence, $p(x,t)$ is uniquely determined by

$$p(x,t) := \left.\frac{\partial u}{\partial \mathbf{n}}\right|_{\partial\Omega}, \tag{4.1}$$

where $\mathbf{n}$ is the outward unit normal to the boundary of Ω at the point $x \in \partial\Omega$. Next, using the Laplace transform of $u(x,t)$, (2.10) and (2.13) one can uniquely determine the function $\tilde{q}(x)$,

$$\tilde{q}(x) := \left.\frac{\partial q}{\partial \mathbf{n}}\right|_{\partial\Omega}. \tag{4.2}$$

In our computations the functions $p(x,t)$, $\tilde{q}(x)$ and $g(x,t)$ are calculated from the solution of the forward problem (3.5) with the exact value of the coefficient $c(x)$. We compute data at the boundary from the numerical solution of the forward problem with the known value of the function $c(x)$. Thus, doing the Laplace transform from the known computed function $u(x,t)$ we smooth out the function q. Our numerical examples and experimental verification of the globally convergent method [18] show that this procedure is stable.

A variational formulation for (3.5) is as follows: for $n = 1,\dots,N$; find $V_n,\ q_n \in H^1(\Omega)$, such that

$$\begin{aligned}\mathcal{F}(q_n, V_n; \varphi) :=& (\nabla q_n, \nabla\varphi) + \left(A_{1,n}\left(k\sum_{i=1}^{n-1}\nabla q_i\right)\nabla q_n, \varphi\right) - (A_{1n}\nabla q_n \nabla V_n, \varphi) + (\varepsilon q_n, \varphi)\\ &+ \left(2\frac{I_{1,n}}{I_0}(\nabla q_n)^2, \varphi\right) - \left(A_{2,n}k^2\left(\sum_{i=1}^{n-1}\nabla q_i(x)\right)^2, \varphi\right)\\ &+ \left(2A_{2,n}\nabla V_n\left(k\sum_{i=1}^{n-1}\nabla q_i\right), \varphi\right) - (A_{2,n}(\nabla V_n)^2, \varphi)\\ \approx& (\tilde{q}_n, \varphi)_{\partial\Omega}, \quad \forall\varphi \in H^1(\Omega).\end{aligned} \tag{4.3}$$

To formulate a corresponding finite-element method for (3.5), we introduce the trial space $W^q_{n,h}$:

$$W^q_{n,h} := \{w_n \in H^1(\Omega) : w_n|_K \in P_1(K), \partial_{\mathbf{n}} w_n|_{\partial\Omega} = \tilde{q}_{n,h}, \forall\, K \in \mathcal{T}_{n,h}\}, \qquad n = 1,\dots,N,$$

where $P_1(K)$ denotes the set of linear functions on K and $\tilde{q}_{n,h}$ is an approximation for $\tilde{q}(x)$. We also introduce the test function space $W_{n,h}$ defined as

$$W_{n,h} := \{w_n : w_n \text{ is continuous on } \Omega, \text{ and } w_n|_K \in P_1(K), \forall K \in \mathcal{T}_{n,h}\}.$$

Note that both $W_{n,h}$ and $W^q_{n,h} \subset H^1(\Omega)$. The finite-element method for (3.5) is now formulated as follows: for $n = 1,\dots,N$, find $q_{n,h}$ and $V_{n,h} \in W^q_{n,h}$, approximations of q_n and V_n, respectively, such that

$$\mathcal{F}(q_{n,h}, V_{n,h}; \varphi) \approx (\tilde{q}_{n,h}, \varphi)_{\partial\Omega}, \quad \forall\,\varphi \in W_{n,h}. \tag{4.4}$$

Subtracting (4.4) from (4.3) we get the classical *Galerkin orthogonality:*

$$\mathcal{F}(q_n, V_n; \varphi) - \mathcal{F}(q_{n,h}, V_{n,h}; \varphi) \approx 0, \quad \forall\,\varphi \in W_{n,h}. \tag{4.5}$$

Now, we introduce the residual, $\mathcal{R}_n := \mathcal{R}_n(q_{nh}, V_{n,h})$, for a discrete solution for (3.5) as follows: for $n = 1,\dots,N$; find $q_{nh}, V_{n,h} \in W^q_{n,h}$ such that

$$\tilde{\mathcal{L}}_{n,\varepsilon}\left(q_{n,h}, V_{n,h}\right) := -\Delta_h q_{nh} + A_{1,n}\left(k\sum_{i=1}^{n-1}\nabla q_{ih}\right)\nabla q_{nh} - A_{1n}\nabla q_{nh}\nabla V_{nh} + \varepsilon q_{nh}$$
$$+ 2\frac{I_{1,n}}{I_0}(q_{nh})^2 - A_{2,n}k^2\left(\sum_{i=1}^{n-1}\nabla q_{ih}(x)\right)^2 + 2A_{2,n}\nabla V_{nh}\left(k\sum_{i=1}^{n-1}\nabla q_{ih}\right)$$
$$- A_{2,n}(\nabla V_{nh})^2 := \mathcal{R}_n, \qquad q_{nh}|_{\partial\Omega} = \tilde{q}, \tag{4.6}$$

where $\Delta_h q_{nh}$ is the discrete Laplacian defined by

$$(\Delta_h q_{nh}, \eta) = (\nabla q_{nh}, \nabla\eta), \qquad \forall\eta \in W_{n,h}. \tag{4.7}$$

Further, we let $e_{n,h} = q_n - q_{n,h}$, $n = 1, \ldots, N$, and then the abstract Galerkin orthogonality relation (4.5) can be written as

$$(\nabla e_{n,h}, \nabla\varphi) + (\varepsilon e_{n,h}, \varphi) + \left(A_{1,n}\left[\left(k\sum_{i=1}^{n-1}\nabla q_i\right)\nabla q_n - \left(k\sum_{i=1}^{n-1}\nabla q_{i,h}\right)\nabla q_{n,h}\right], \varphi\right)$$
$$- (A_{1n}[\nabla q_n\nabla V_n - \nabla q_{n,h}\nabla V_{n,h}], \varphi) + \left(2\frac{I_{1,n}}{I_0}[(\nabla q_n)^2 - (\nabla q_{n,h})^2], \varphi\right)$$
$$- \left(A_{2,n}k^2\left[\left(\sum_{i=1}^{n-1}\nabla q_i(x)\right)^2 - \left(\sum_{i=1}^{n-1}\nabla q_{i,h}(x)\right)^2\right], \varphi\right)$$
$$+\left(2A_{2,n}\left[\nabla V_n\left(k\sum_{i=1}^{n-1}\nabla q_i\right) - \nabla V_{n,h}\left(k\sum_{i=1}^{n-1}\nabla q_{i,h}\right)\right], \varphi\right)$$
$$- (A_{2,n}[(\nabla V_n)^2 - (\nabla V_{n,h})^2, \varphi)]$$
$$:= (\nabla e_{n,h}, \nabla\varphi) + (\varepsilon e_{n,h}, \varphi) + \sum_{j=1}^{6}(T_j, \varphi) \approx 0, \qquad \forall\varphi \in W_{n,h}, \tag{4.8}$$

with the obvious notations for T_j, $j = 1, \ldots, 6$. Now subtracting (4.6) from (4.8), we get the error equation

$$-\Delta_h e_{n,h} + \varepsilon e_{n,h} + \sum_{j=1}^{6} T_j := -\mathcal{R}_n. \tag{4.9}$$

Thus, (4.8) can be written as an equation with the right-hand side $-(\mathcal{R}_n, \varphi)$. Below, to keep a track of contributions from the q and V in (4.9), we rearrange the mixed q- and V-terms: T_1, T_2 and T_5:

$$T_1 = A_{1,n}k\left[\left(\sum_{i=1}^{n-1}\nabla q_i\right)\nabla q_n - \left(\sum_{i=1}^{n-1}\nabla q_{i,h}\right)\nabla q_{n,h}\right]$$
$$+ A_{1,n}k\left[\left(\sum_{i=1}^{n-1}\nabla q_{i,h}\right)\nabla q_n - \left(\sum_{i=1}^{n-1}\nabla q_{i,h}\right)\nabla q_n\right]$$
$$= A_{1,n}k\left(\sum_{i=1}^{n-1}\nabla q_{i,h}\right)\cdot\nabla e_{n,h} + A_{1,n}k\nabla q_n\left(\sum_{i=1}^{n-1}\nabla e_{i,h}\right). \tag{4.10}$$

Similarly we rearrange the term T_2 on the left-hand side of (4.9) as

$$-T_2 = A_{1n}[\nabla q_n\nabla V_n - \nabla q_{n,h}\nabla V_{n,h}] + A_{1n}\nabla q_n\nabla V_{n,h} - A_{1n}\nabla q_n\nabla V_{n,h}$$
$$= A_{1n}\nabla q_n\nabla\Theta_n + A_{1n}\nabla V_{n,h}\nabla e_{n,h}, \tag{4.11}$$

where we have defined $\Theta_n := V_n - V_{n,h}$. Finally, T_5 is written as

$$T_5 = 2kA_{2,n}\left[\nabla V_n\left(\sum_{i=1}^{n-1}\nabla q_i\right) - \nabla V_{n,h}\left(\sum_{i=1}^{n-1}\nabla q_{i,h}\right)\right]$$
$$+\ 2kA_{2,n}\left[\nabla V_{n,h}\left(\sum_{i=1}^{n-1}\nabla q_i\right) - \nabla V_{n,h}\left(\sum_{i=1}^{n-1}\nabla q_i\right)\right]$$
$$= 2kA_{2,n}\left(\sum_{i=1}^{n-1}\nabla q_i\right)\nabla\Theta_n + 2kA_{2,n}\nabla V_{n,h}\left(\sum_{i=1}^{n-1}\nabla e_{i,h}\right).$$

Substituting rearranged terms into (4.9) yields

$$-\Delta_h e_{n,h} + I_1\nabla e_{n,h} + \varepsilon e_{n,h} + 2\frac{I_{1,n}}{I_0}[(\nabla q_n)^2 - (\nabla q_{n,h})^2]$$
$$+ I_2\cdot\left(k\sum_{i=1}^{n-1}\nabla e_{i,h}\right) + I_3\cdot\nabla\Theta_n = -\mathcal{R}_n, \tag{4.12}$$

where

$$I_1 = A_{1,n}\left(k\left(\sum_{i=1}^{n-1}\nabla q_i\right) - \nabla V_{n,h}\right),$$
$$I_2 = \left(A_{1n}\nabla q_n - A_{2,n}k\sum_{i=1}^{n-1}(\nabla q_{i,h} + \nabla q_i) + 2A_{2,n}\nabla V_{n,h}\right) \tag{4.13}$$
$$I_3 = \left(2kA_{2,n}\left(\sum_{i=1}^{n-1}\nabla q_i\right) - A_{1n}\nabla q_n - A_{2,n}(\nabla V_{n,h} + \nabla V_n)\right).$$

Below we give (Lipschitz) bounds for the coefficients I_1, I_2, I_3 (see also [3], section 3.1).

Lemma 4.1. *Let $0 < \alpha < 1$ be the Lipschitz order. Assume that*

$$\max_{1\leqslant n\leqslant N}|q_n^*|_{1+\alpha} \leqslant C^*, \qquad |V_{n,h}|_{1+\alpha} \leqslant \xi \tag{4.14}$$

where the constant $C^* = C^*(\|q^*\|_{C^{2+\alpha}(\overline{\Omega})\times C^1[\underline{s},\bar{s}]}) > 1$. Then we have the following Lipschitz bounds:

$$|I_1|_\alpha + |I_2|_\alpha + |I_3|_\alpha \leqslant 3M^*(1+\beta+\eta) \tag{4.15}$$

$$\left|I_2\cdot\left(k\sum_{i=1}^{n-1}\nabla e_{i,h}\right)\right|_\alpha + |I_3\cdot\nabla\Theta_n|_\alpha \leqslant 3M^*\eta. \tag{4.16}$$

Proof. From (3.8), the definition of β, (4.14) and the fact that $C^* \geqslant 1$, it follows that

$$|I_1|_\alpha \leqslant |A_{1,n}|\left|k\left(\sum_{i=1}^{n-1}\nabla q_i\right) - \nabla V_{n,h}\right|_\alpha \leqslant 8\bar{s}^2\Big(kN|q_n|_{1+\alpha} + |V_{n,h}|_{1+\alpha}\Big)$$
$$\leqslant 8\bar{s}^2(\beta C^* + \xi) \leqslant 8\bar{s}^2(\beta C^* + \eta/2) \leqslant \frac{1}{2}M^*(\beta+\eta) \tag{4.17}$$

and

$$|I_2|_\alpha \leqslant \left| A_{1,n}\nabla q_n - A_{2,n}k\sum_{i=1}^{n-1}\left(\nabla q_{i,h} + \nabla q_i\right) + 2A_{2,n}\nabla V_{n,h}\right|_\alpha$$
$$\leqslant 8\bar{s}^2(C^* + 2\beta C^* + 2\xi) \leqslant \frac{M^*}{2}(1 + 2\beta + \eta) = M^*\left(\beta + \frac{1}{2} + \frac{\eta}{2}\right). \tag{4.18}$$

Now (4.15) is a result of combining (4.17), (4.18) and the following estimate for $|I_3|_\alpha$:

$$|I_3|_\alpha = \left|2A_{2,n}k\sum_{j=1}^{n-1}\nabla q_i - A_{1,n}\nabla q_n - A_{2,n}\left(\nabla V_{n,h} + \nabla V_n\right)\right|_\alpha \leqslant M^*\left(\beta + \frac{1}{2} + \frac{\eta}{2}\right). \tag{4.19}$$

To prove the second assertion of the lemma we use the shift theorem, an interpolation estimate and Poincaré inequality to write

$$|q_{n,h} - q_n|_{1+\alpha} \leqslant |q_{n,h} - q_n^\star|_{1+\alpha} + |q_n^\star - q_n|_{1+\alpha} \leqslant k|q_n^\star|_{2+\alpha} + |q_n^\star - q_n|_{2+\alpha},$$

and we have by (3.11),

$$k\sum_{i=1}^{n-1}\left|\nabla e_{i,h}\right|_\alpha \leqslant k^2\sum_{i=1}^{n-1}\left|q_n^\star\right|_{2+\alpha} + k\sum_{i=1}^{n-1}\left|q_{n,i} - q_n^*\right|_{2+\alpha} \leqslant 2(k+K)M^*\beta\left(\frac{1}{\sqrt{\lambda}} + 3\eta\right). \tag{4.20}$$

Hence, using the Hölder inequality

$$|f_1 f_2|_\alpha \leqslant |f_1|_\alpha\,|f_2|_\alpha\,, \qquad \forall f_1,\ f_2 \in C(\bar{\Omega}) \tag{4.21}$$

and the estimates (4.18) and (4.20) we get

$$\left|I_2 \cdot k\sum_{j=1}^{n-1}\nabla e_{i,h}\right|_\alpha \leqslant |I_2|_\alpha\, k\sum_{j=1}^{n-1}\left|\nabla e_{i,h}\right|_\alpha \leqslant (k+K)(M^\star)^2\beta\,(1+2\beta+\eta)\left(\frac{1}{\sqrt{\lambda}} + 3\eta\right). \tag{4.22}$$

Further by (3.9), (4.19) and the definition of η,

$$|I_3 \cdot \nabla\Theta_n|_\alpha \leqslant |I_3|_\alpha\,|\nabla\Theta_n|_\alpha \leqslant M^*\left(\beta + \frac{1}{2} + \frac{\eta}{2}\right)\frac{\eta}{2}. \tag{4.23}$$

Thus, using (3.11),

$$\left|I_2 \cdot k\sum_{j=1}^{n-1}\nabla e_{i,h}\right|_\alpha + |I_3 \cdot \nabla\Theta_n|_\alpha \leqslant M^*(1+2\beta+\eta)\left[\frac{\eta}{2} + (k+K)M^\star\beta\left(\frac{1}{\sqrt{\lambda}} + 3\eta\right)\right]. \tag{4.24}$$

Now since $\beta \leqslant 1/(24KM^\star)$ and $\frac{1}{\sqrt{\lambda}} \leqslant \eta$ we get

$$\left[\frac{\eta}{2} + (k+K)M^\star\beta\left(\frac{1}{\sqrt{\lambda}} + 3\eta\right)\right] \leqslant \eta\left(\frac{1}{2} + 4(k+K)M^\star\beta\right) \leqslant \eta\left(\frac{1}{2} + \frac{1}{3}\right) = \frac{5}{6}\eta < \eta. \tag{4.25}$$

Recall that $\eta \leqslant 1/(16KM^\star)$ and by (3.4) and (3.8), $C^* \geqslant 1$ and $\bar{s} \geqslant 1$; thus, by (3.8) $M^\star \geqslant 16$. Hence,

$$M^\star(1+2\beta+\eta) \leqslant M^\star + \frac{7}{48K} \leqslant 3M^\star. \tag{4.26}$$

Finally

$$M^*(1+2\beta+\eta)\left[\eta + KM^\star\beta\left(\frac{1}{\sqrt{\lambda}}+3\eta\right)\right] \leqslant 3M^\star\eta = 3M^\star\eta, \tag{4.27}$$

which gives the desired result and the proof is complete. □

Our estimates take place in finite-dimensional spaces and therefore they are involved in L_2-based norms which are equivalent with those based on Hölder norms. Since the coefficients $I_i, i = 1, 2, 3$, in (4.12) are Lipschitz continuous, we may restate (4.12) with the continuous Laplacian. We rewrite (4.12) for every pseudo-frequency interval $[s_n, s_{n-1})$ for all $n = 1, \ldots, N$ (we suppress the index n) and consider an error equation

$$\Gamma e := -\Delta e + C_1\nabla e + \varepsilon e + \delta\Lambda e = -C_2\Big(k\sum_{i=1}^{n-1}\nabla e_i\Big) - \mathcal{R} - C_3\nabla\Theta := -\tilde{\mathcal{R}} - C_3\nabla\Theta, \tag{4.28}$$

$$e|_{\partial\Omega} = 0,$$

with $\mathcal{R}$ being the dominating part of $\tilde{\mathcal{R}}$, C_j, $j = 1, 2, 3$, corresponding to the spatially continuous versions of I_j:s, $\delta := I_{1,n}/I_0$ and Λ the nonlinear term defined by

$$\Lambda e := |\nabla q|^2 - |\nabla q_h|^2. \tag{4.29}$$

Observe that in (4.28) the sum is over all the previous iteration steps in the pseudo-frequency interval and the error in V is included in the Θ-term.

Note that by (4.8) and (4.9) we have that the residual term $\mathcal{R}$ satisfies

$$(\mathcal{R}, \varphi) \approx 0, \qquad \forall\varphi \in W_{n,h}; \tag{4.30}$$

in other words, the residual $\mathcal{R}(q_h)$ is almost orthogonal ($\sim\perp$) to the finite-element space $W_{n,h}$.

5. Bounds for the nonlinear operator Λ and *a priori* estimates

Below first we shall derive some bounds for the nonlinear operator Λ. To this end let $f(q) = |\nabla q|^2$ and $0 < \theta < 1$; then, Taylor expanding $f(q_h)$ about q we may write

$$f(q_h) = f(q) + (q_h - q)\mathcal{D}f(\theta q + (1-\theta)q_h), \tag{5.1}$$

where $\mathcal{D}$ is the differential operator and

$$\begin{aligned}\mathcal{D}f(\theta q + (1-\theta)q_h) &= \mathcal{D}(|\nabla(\theta q + (1-\theta)q_h)|^2)\\ &= 2(|\nabla(\theta q + (1-\theta)q_h)|)\cdot(\mathcal{D}|\nabla(\theta q + (1-\theta)q_h)|).\end{aligned} \tag{5.2}$$

Thus, we may write Λe in the concise form as

$$\begin{aligned}\Lambda e &= 2e(|\theta\nabla e + \nabla q_h|)\cdot(\mathcal{D}|\nabla(\theta q + (1-\theta)q_h)|)\\ &= 2e(|\theta\nabla e + \nabla q_h|)\cdot(\mathcal{D}|\theta\nabla e + \nabla q_h|).\end{aligned} \tag{5.3}$$

When approximating with piecewise linear q_h, it is more adequate to use the first equality in (5.3).

5.1. The dual problem for a linearized approach

In this part we briefly sketch a framework for the dual approach for a *linear/linearized version* of (4.28). For a more detailed study (in a one-dimensional case) we refer to [11]. To begin with, we assume that Λ is a linear operator and let

$$\Gamma^\star\varphi := -\Delta\varphi - C_1\nabla\varphi + \varepsilon\varphi + \delta\Lambda^\star\varphi = e, \qquad n = 1, \ldots, N, \qquad \varphi|_{\partial\Omega} = 0, \tag{5.4}$$

with $\Gamma^\star$ and $\Lambda^\star$ being the adjoints of Γ and Λ, respectively. By (4.28) we have *the error representation formula*

$$\|e\|^2_{L_2(\Omega)} = (e, \Gamma^\star\varphi) = (\Gamma e, \varphi) = -(\tilde{\mathcal{R}}, \varphi). \tag{5.5}$$

Further, we use identities

$$\begin{aligned} &-(\chi, \varphi - P_h\varphi) = -(\chi - P_h\chi, \varphi - P_h\varphi) \qquad \text{for} \\ &\chi = \mathcal{R}, \qquad \chi = C_2 \sum_{i=1}^{n-1} \nabla e_i \qquad \text{or} \quad \chi = C_3 \nabla\Theta, \end{aligned} \tag{5.6}$$

where $P_h : L_2(\Omega) \to W_{n,h}$ is the $L_2(\Omega)$-projection, and we have used the orthogonality $\mathcal{R} \perp W_{n,h}$ and $(\varphi - P_h\varphi) \perp W_{n,h}$. Finally, combining the interpolation estimate

$$\|h^{-2}(\varphi - P_h\varphi)\|_{L_2(\Omega)} \leqslant C_i \|D^2\varphi\|_{L_2(\Omega)} \tag{5.7}$$

and the strong stability estimate for the dual problem (5.4)

$$\|D^2\varphi\|_{L_2(\Omega)} \leqslant C_s \|e\|_{L_2(\Omega)}, \tag{5.8}$$

we get from (5.5) and with the fact that $\mathcal{R}$ dominates $\tilde{\mathcal{R}}$ that

$$\|e\|_{L_2(\Omega)} \leqslant C_s C_i \|h^2(\tilde{\mathcal{R}} - P_h\tilde{\mathcal{R}})\| \leqslant C C_s C_i \|h^2(\mathcal{R} - P_h\mathcal{R})\|, \tag{5.9}$$

where C_i and C_s are interpolation and stability constants, respectively. Recalling (5.3) we have

$$(\Lambda^\star\varphi, e) = (\varphi, \Lambda e) = 2(\varphi, [|\theta\nabla e + \nabla q_n|] \cdot [\mathcal{D}|\nabla(\theta q + (1-\theta)q_h)|]e). \tag{5.10}$$

Assuming the piecewise linear approximation by successive application of the Hölder inequality we get

$$\begin{aligned} |(\Lambda^\star\varphi, e)| &= |(\varphi, \Lambda e)| = 2|(\varphi, [|\theta\nabla e + \nabla q_h|] \cdot [\mathcal{D}|\nabla(\theta q + (1-\theta)q_h)|]e)| \\ &\leqslant 2\theta|(\varphi, |\nabla q_h|\mathcal{D}(|\nabla q|)e)| + 2\theta^2|(\varphi, |\nabla e|\mathcal{D}(|\nabla q|)e)| \\ &\leqslant 2\theta\|q_h\|_{W^1_\infty}\|\varphi\|\|e\|\|q\|_{W^2_\infty} + 2\theta^2\|\varphi\|\|e\|\|e\|_{W^1_\infty}\|q\|_{W^2_\infty} \\ &\leqslant C\|\varphi\|\|e\|\|q\|_{W^2_\infty}(\|q_h\|_{W^1_\infty} + \|e\|_{W^1_\infty}). \end{aligned} \tag{5.11}$$

Here we used the fact that

$$\begin{aligned} \mathcal{D}|\nabla(\theta q + (1-\theta)q_h)| &= \mathcal{D}(\theta|\nabla q| + (1-\theta)|\nabla q_h|) \\ &= \theta\mathcal{D}(|\nabla q|) + (1-\theta)D(|\nabla q_h|) = \theta\mathcal{D}(|\nabla q|). \end{aligned} \tag{5.12}$$

Thus, we get the following estimate for the nonlinear operator Λ:

$$\|\Lambda\| \leqslant \|q\|_{W^2_\infty}\big(\|q_h\|_{W^1_\infty} + \|e\|_{W^1_\infty}\big).$$

As an alternative method to get the above-derived estimate we can apply a direct approach using the definition $\Lambda e = |\nabla q|^2 - |\nabla q_h|^2$. This definition yields a weak bound for Λ (or Λ^*):

$$\begin{aligned} |(\Lambda^\star\varphi, e)| &= |(\varphi, \Lambda e)| = |(\varphi, |\nabla q|^2 - |\nabla q_h|^2)| = |(\varphi, (|\nabla q| - |\nabla q_h|)(|\nabla q| + |\nabla q_h|))| \\ &\leqslant |(\varphi, |\nabla(q - q_h)|(|\nabla q| + |\nabla q_h|))| = |(\varphi, |\nabla e|(|\nabla q| + |\nabla q_h|))| \\ &\leqslant \|\varphi\|\|e\|_{W^1_2}(\|q\|_{W^1_\infty} + \|q_h\|_{W^1_\infty}). \end{aligned} \tag{5.13}$$

Theorem 5.1 (An *a priori* error bound)**.** *Let $q_n \in W^2_2(\Omega)$ and q_{nh} be the solutions for (4.3) and (4.4), respectively. Then for a piecewise linear finite-element approximation error $e_n = q_n - q_{n,h}$ we have*

$$\|e_n\| \leqslant Ch\|q_n\|_{W^2_2} = \mathcal{O}(h). \tag{5.14}$$

Proof. We use the Taylor expansion with a second-order rest term (corresponding to $\theta = 0$ in (5.3))

$$f(q) = f(q_h) + (q - q_h) f'(q_h) + r, \qquad r = \mathcal{O}(q - q_h)^2, \tag{5.15}$$

where we have suppressed n. Thus,

$$|\nabla q|^2 \approx |\nabla q_h|^2 + (q - q_h) \cdot 2|\nabla q_h| \mathcal{D}(|\nabla q_h|) \tag{5.16}$$

and

$$\Lambda e = |\nabla q|^2 - |\nabla q_h|^2 \approx 2e \cdot |\nabla q_h| \mathcal{D}(|\nabla q_h|). \tag{5.17}$$

Hence,

$$(\Lambda^\star \varphi, e) = (\varphi, \Lambda e) \approx 2(\varphi, e \cdot |\nabla q_h| \mathcal{D}(|\nabla q_h|)) = 2(e\varphi |\nabla q_h|, \mathcal{D}(|\nabla q_h|)) \tag{5.18}$$

and

$$\begin{aligned}(e\varphi |\nabla q_h|, \mathcal{D}(|\nabla q_h|)) &= -(|\nabla q_h|, \mathcal{D}(e\varphi |\nabla q_h|)) + (|\mathbf{n} \cdot \nabla q_h|, e\varphi |\nabla q_h|)|_{\partial\Omega} \\ &= -(|\nabla q_h|, e\varphi \mathcal{D}(|\nabla q_h|)) - (|\nabla q_h|, e\mathcal{D}(\varphi) |\nabla q_h|) \\ &\quad - (|\nabla q_h|, \mathcal{D}(e)\varphi |\nabla q_h|),\end{aligned} \tag{5.19}$$

where due to the fact that $e \equiv 0$ at the boundary, the contribution from the boundary term vanishes. By rearranging the terms we get an approximation (with an error of order r, see (5.15))

$$(\varphi, \Lambda e) \approx -(|\nabla q_h|\,, e\mathcal{D}(\varphi)\,|\nabla q_h|) - (|\nabla q_h|\,, \mathcal{D}(e)\varphi\,|\nabla q_h|). \tag{5.20}$$

Let now $\tilde{q}$ be an interpolant of q. Then, using the split $e = q - \tilde{q} + \tilde{q} - q_h$ and the Galerkin orthogonality (4.8) together with the stability estimate (4.10) we may write

$$\begin{aligned}\|e\|^2 = (e, e) &= (\Gamma^\star \varphi, e) = (\Delta\varphi, e) - (C_1 \nabla\varphi, e) - (\varepsilon\varphi, e) - (\Lambda^* \varphi, e) \\ &= (D^2\varphi, \nabla(q - \tilde{q})) - (C_1\nabla\varphi, q - \tilde{q}) - (\varepsilon\varphi, q - \tilde{q}) - (\Lambda^*\varphi, q - \tilde{q}) \\ &\leqslant C_i h^2 \big(C_s \|e\|_{L_2} + C_1 \|\varphi\|_{W_2^1} + (\varepsilon + \|\Lambda^*\|)\|\varphi\|\big)\|q\|_{W_2^2}.\end{aligned} \tag{5.21}$$

Thus, we have obtained following the *a priori* error bound

$$\|e\| \leqslant Ch\|q\|_{W_2^2} = \mathcal{O}(h). \tag{5.22}$$

□

Remark 2. Since we assumed q_h to be a linear approximation, in the Taylor formula (5.13) the rest term r contains $f''(q_h) = \mathcal{D}^2(\frac{1}{2}|\nabla q_h|^2) \equiv 0$. Then, in the above proof all approximation signs $\approx$ can be replaced by $=$. With the $\approx$, the argument holds for the higher order approximation.

6. *A posteriori* error estimation

The *a posteriori* error analysis is based on representing the error in terms of the solution φ of the dual problem related to (3.5). We recall the problem (4.28) and write the dual problem for all $[s_n, s_{n-1})$:

$$-\Delta\varphi - C_1\nabla\varphi + \varepsilon\varphi + \delta\Lambda^\star\varphi + \delta\,|\nabla\varphi_h|^2 + \tilde{C}_{\varphi,\Theta} = \psi, \qquad n = 1, \ldots, N, \qquad \varphi|_{\partial\Omega} = 0, \tag{6.1}$$

where $\tilde{C}_{\varphi,\Theta} := C_2 k \sum_{i=1}^{n-1} \nabla\varphi_i + C_3\nabla\Theta$ is considered to be known from the previous iteration steps, and $\Theta = \Theta_n = V_h - V_{n,h}$. We assume that $\Theta \in H^1_{\mathrm{loc}}$ and $\varphi_h \in W^{1,4}_{\mathrm{loc}}$ (this corresponds to global assumptions: $V \in H^2(\Omega)$ and $\varphi \in W_4^2(\Omega)$). Note, that we have added an extra

term $\delta\,|\nabla\varphi_h|^2$ to the dual problem (6.1) because of the presence of the nonlinear term $\Lambda e = |\nabla q|^2 - |\nabla q_h|^2$ to keep the continuity of our problem. Thus, we wish to control the quantity (e, ψ) with $e = q - q_h$ in Ω, where $\psi \in [L^2(\Omega)]^3$ is given. For approximations of spectral order >1 (for linear approximation the J_5-term below will vanish), using (5.20) we may write

$$\begin{aligned}(\psi, e) &= -(\Delta\varphi, e) - (C_1\nabla\varphi, e) + (\varepsilon\varphi, e) + \delta(\varphi, \Lambda e) + \delta(|\nabla\varphi_h|^2, e) + (\tilde{C}_{\varphi,\Theta}, e)\\ &\approx -(\Delta\varphi, e) - (C_1\nabla\varphi, e) + (\varepsilon\varphi, e) - \delta(|\nabla q_h|^2\,\mathcal{D}(\varphi), e) + \delta(\mathcal{D}(|\nabla q_h|^2\,\varphi), e)\\ &\quad + \delta(|\nabla\varphi_h|^2, e) + (\tilde{C}_{\varphi,\Theta}, e) := J_1 + J_2 + J_3 + J_4 + J_5 + J_6 + J_7. \qquad (6.2)\end{aligned}$$

Due to the limited regularity of the approximate solution $q_{n,h}$, the scalar products I_j, $j = 1, \ldots, 7$, involving $e = q_n - q_{n,h}$ should be performed elementwise: $(f, g) := \sum_K (f, g)_K$. This will introduce the accumulative sum of the normal derivatives over the element boundaries. Taking into account these boundary terms and using the Green's formula, we recompute each J_j, $j = 1, \ldots, 7$, separately:

$$\begin{aligned}J_1 = -(\Delta\varphi, e) &= (\nabla\varphi, \nabla e) - \sum_K \int_{\partial K} (\partial_{\mathbf{n}}\varphi) e\,\mathrm{d}s\\ &= -\sum_K \int_{\partial K} (\partial_{\mathbf{n}}\varphi) e\,\mathrm{d}s + \sum_K \int_{\partial K} (\partial_{\mathbf{n}} e)\varphi\,\mathrm{d}s - (\Delta_h e, \varphi), \qquad (6.3)\end{aligned}$$

where Δ_h is the discrete Laplacian and $\partial_{\mathbf{n}} f := \mathbf{n}\cdot\nabla f$ denote the normal derivative of f in the direction of the outward unit normal $\mathbf{n}$ to the boundary ∂K of element K. As for J_2 integrating by parts, and using the facts that (i) the minimum regularity requirement for elements in $\tilde{V}_h$ is C^1, (ii) the oriented integrals over the element boundaries ∂K such that $\partial K \cap \partial\Omega = \emptyset$ cancels out, and finally (iii) $e \equiv 0$ on $\partial\Omega$, componentwise integration, yields

$$J_2 = -(C_1\nabla\varphi, e) = (C_1\nabla e, \varphi) - C_1 \sum_K \int_{\partial K} \varphi e\,\mathrm{d}s = (C_1\nabla e, \varphi). \qquad (6.4)$$

Next, we leave the terms J_3, J_6 and J_7 in their present form, namely

$$J_3 + J_6 + J_7 = (\varepsilon e, \varphi) + (e, \tilde{C}_{\varphi,\Theta}) + \delta(e, |\nabla\varphi_h|^2). \qquad (6.5)$$

Finally, the remaining contribution from the nonlinear terms J_4 and J_5 can be rewritten as

$$\begin{aligned}J_4 + J_5 &= -\delta(|\nabla q_h|^2\,\mathcal{D}(\varphi), e) + \delta(\mathcal{D}(|\nabla q_h|^2\,\varphi), e)\\ &= -\delta \sum_K \int_{\partial K} |\nabla q_h|^2\,\varphi e\,\mathrm{d}s + \delta(\varphi, \mathcal{D}(|\nabla q_h|^2\, e))\\ &\quad + \delta \sum_K \int_{\partial K} |\nabla q_h|^2\,\varphi e\,\mathrm{d}s - \delta(\varphi, |\nabla q_h|^2\,\mathcal{D}e)\\ &= \delta(\varphi, \mathcal{D}(|\nabla q_h|^2\, e)) - \delta(\varphi, |\nabla q_h|^2\,\mathcal{D}e). \qquad (6.6)\end{aligned}$$

Substituting (6.3)–(6.6) into equation (6.2), using (5.20), and finally recalling (4.28), we get

$$\begin{aligned}(\psi, e) &= -\sum_K \int_{\partial K} (\partial_{\mathbf{n}}\varphi) e\,\mathrm{d}s + \sum_K \int_{\partial K} (\partial_{\mathbf{n}} e)\varphi\,\mathrm{d}s - (\varphi, \Delta_h e) + (C_1\nabla e, \varphi) + (\varepsilon e, \varphi)\\ &\quad + (e, \tilde{C}_{\varphi,\Theta}) + \delta(e, |\nabla\varphi_h|^2) + \delta(\varphi, \mathcal{D}(|\nabla q_h|^2\, e)) - \delta(\varphi, (|\nabla q_h|^2\,\mathcal{D}e))\\ &= -(\Delta_h e - C_1\nabla e - \varepsilon e - \delta\Lambda e, \varphi) + (e, \tilde{C}_{\varphi,\Theta}) + \delta(e, |\nabla\varphi_h|^2)\\ &\quad - \sum_K \int_{\partial K} (\partial_{\mathbf{n}}\varphi) e\,\mathrm{d}s + \sum_K \int_{\partial K} (\partial_{\mathbf{n}} e)\varphi\,\mathrm{d}s\end{aligned}$$

$$= (-\tilde{\mathcal{R}}, \varphi) + C_3(e, \nabla\Theta) + \delta(e, |\nabla\varphi_h|^2) - \sum_K \int_{\partial K} (\partial_{\mathbf{n}}\varphi) e \, \mathrm{d}s + \sum_K \int_{\partial K} (\partial_{\mathbf{n}} e)\varphi \, \mathrm{d}s. \tag{6.7}$$

We estimate the boundary terms in (6.7) as follows: first, the sum over the element boundaries, where each interior side $S \in S_h$ occurs twice. Then denoting by $\partial_{\mathbf{n}^\pm}\vartheta$ the derivative of ϑ in the outward normal direction $\mathbf{n}^\pm$ to the element $K^\pm$, and by $\partial_s\vartheta$ the derivative of a function ϑ in one of the normal directions, $\mathbf{n}^-$ and $\mathbf{n}^+$, of each side S we may write

$$\sum_K \int_{\partial K} (\partial_{\mathbf{n}}\vartheta)\varphi \, \mathrm{d}s = \sum_S \int_S [\partial_s\vartheta]\varphi \, \mathrm{d}s, \tag{6.8}$$

where $\left[\partial_s\vartheta\right]$ denotes the jump across the side $S \subset \partial K$ defined by

$$[\partial_s\vartheta] = \max_{S\in\partial K}\{\partial_{\mathbf{n}^+}\vartheta, \partial_{\mathbf{n}^-}\vartheta\}.$$

A uniform distribution of each jump on to the two faces of a common side S for two adjacent elements yields

$$\sum_S \int_S [\partial_s\vartheta]\,\varphi \, \mathrm{d}s = \sum_K \frac{1}{2} \int_{\partial K} [\partial_s\vartheta]\varphi \, \mathrm{d}s. \tag{6.9}$$

Next we, formally, set $\mathrm{d}x = h_K \mathrm{d}s$ and replace the integrals over the element boundaries ∂K by integrals over the elements K to get

$$\left| \sum_K \frac{1}{2} h_K^{-1} \int_{\partial K} [\partial_s\vartheta]\varphi h_K \, \mathrm{d}s \right| \leqslant C \int_\Omega \max_{S\subset\partial K} h_K^{-1} |[\partial_s\vartheta]|_K ||\varphi| \, \mathrm{d}x, \tag{6.10}$$

where $[\partial_s\vartheta]|_K = \max_{S\subset\partial K}[\partial_s\vartheta]|_S$. Now for the error e we recognize that we have

$$[\partial_s e]|_K = [\partial_s(q - q_h)]|_K = [\partial_s q_h]|_K. \tag{6.11}$$

Assuming continuously differentiable φ, the sum involving the jumps $[\partial_{\mathbf{n}}\varphi]$ vanish automatically. Hence, using (6.11) the contribution from the boundary term involving $\partial_{\mathbf{n}} e$ can be estimated as

$$\left| \sum_K \frac{1}{2} h_K^{-1} \int_{\partial K} [\partial_s e]\varphi h_K \, \mathrm{d}s \right| \leqslant C \int_\Omega \max_{S\subset\partial K} h_K^{-1} |[\partial_s q_h]||\varphi| \, \mathrm{d}x. \tag{6.12}$$

Finally, substituting the estimate (6.12) into (6.7), we end up with

$$|(\psi, e)| \leqslant (|\tilde{\mathcal{R}}|, |\varphi|) + C_3(|\nabla\Theta|, |e|) + \delta(|\nabla\varphi_h|^2, |e|) + C\big(\max_{S\subset\partial K} h_K^{-1}|[\partial_s q_h]|, |\varphi|\big).$$

Next, we use the splitting

$$\varphi - \varphi_h = \big(\varphi - \varphi_h^I\big) + \big(\varphi_h^I - \varphi_h\big),$$

where $\varphi_h^I \in U_h$ denotes an interpolant of φ, and using the Galerkin orthogonality (4.8) we have

$$(|\tilde{\mathcal{R}}|, |\varphi|) + C\big(\max_{S\subset\partial K} h_K^{-1}|[\partial_s q_h]|, |\varphi|\big) \leqslant \big(|\tilde{\mathcal{R}}|, \big|\varphi - \varphi_h^I\big|\big) + C\big(\max_{S\subset\partial K} h_K^{-1}|[\partial_s e]|, \big|\varphi - \varphi_h^I\big|\big). \tag{6.13}$$

Now, we use the following standard, elementwise, interpolation estimate:

$$\big\|\varphi - \varphi_h^I\big\|_{L_p(K)} \leqslant C h_K^2 \|\mathcal{D}^2\varphi\|_{L_p(K)}, \qquad p = 1, 2, \infty. \tag{6.14}$$

We may approximate the second spatial derivative as, see [11],

$$\mathcal{D}^2\varphi \approx \frac{[\partial_{\mathbf{n}}\varphi_h]}{h_K}. \tag{6.15}$$

Substituting (6.15) in (6.14) yields an interpolation error as

$$\left|\varphi - \varphi_h^I\right| \leqslant Ch_K|[\partial_{\mathbf{n}}\varphi_h]|. \tag{6.16}$$

Inserting the estimates (6.11) and (6.16) in (6.13) we get

$$\begin{aligned}(|\tilde{\mathcal{R}}|, |\varphi|) + C\Big(\max_{S\subset\partial K} h_K^{-1}|[\partial_s q_h]|, |\varphi|\Big) &\leqslant C(|\tilde{\mathcal{R}}|, h_K|[\partial_{\mathbf{n}}\varphi_h]|)\\ &+ C\Big(\max_{S\subset\partial K} h_K^{-1}|[\partial_s q_h]|, h_K|[\partial_{\mathbf{n}}\varphi_h]|\Big).\end{aligned}$$

In this way we have derived the following error representation inequality.

Lemma 6.1. *Let φ be the solution of the dual problem (6.1), q the solution of (4.3) and q_h the FEM approximated solution of (4.4). Then the following error representation inequality holds true:*

$$|(\psi, e)| \leqslant (|\tilde{\mathcal{R}}_1|, |\sigma|) + (|\tilde{\mathcal{R}}_2|, |\sigma|) + C_3(|\nabla\Theta|, |e|) + \delta(|\nabla\varphi_h|^2, |e|), \tag{6.17}$$

where the residuals are defined as

$$\tilde{\mathcal{R}}_1 := \tilde{\mathcal{R}}(e) = \Delta_h e - C_1\nabla e - \varepsilon e - \delta\Lambda e - C_2 k\sum_{i=1}^{n-1}\nabla e_i, \qquad \tilde{\mathcal{R}}_2 = \max_{S\subset\partial K} h_K^{-1}|[\partial_s q_h]|, \tag{6.18}$$

and the interpolation error is

$$\sigma = h_K[\partial_{\mathbf{n}}\varphi_h]. \tag{6.19}$$

Now we use, elementwise, the Hölder inequality and estimates of type (6.16) to obtain

$$\begin{aligned}|(\psi, e)| &\leqslant \left(|\mathcal{R}|, \left|\varphi - \varphi_h^I\right|\right) + C\Big(\max_{S\subset\partial K} h_K^{-1}|[\partial_s e]|, \left|\varphi - \varphi_h^I\right|\Big) + C_3(|\nabla\Theta|\,, |e|) + \delta(|\nabla\varphi_h|^2\,, |e|)\\ &\leqslant \sum_K \|h_K\mathcal{R}\|_{L_2(K)} \left\|h_K^{-1}(\varphi - \varphi_h^I)\right\|_{L_2(K)}\\ &\quad + |C_3|\sum_K \|\nabla\Theta\|\,\|e\| + |\delta|\sum_K \|\nabla\varphi_h\|_{L_4(K)}^2\,\|e\|\\ &\quad + C\Big(\max_{S\subset\partial K} h_K^{-1}\Big)\sum_K \|h_K[\partial_s e]\|_{L_2(\partial K)} \left\|h_K^{-1}(\varphi - \varphi_h^I)\right\|_{L_2(K)}\\ &\leqslant \sum_K \|h_K\mathcal{R}\|_{L_2(K)} \sum_K \|[\partial_{\mathbf{n}}\varphi]\|_{L_2(\partial K)} + C|C_3|^2\sum_K \|\nabla\Theta\|_{L_2(K)}^2\\ &\quad + \frac{1}{4}\|e\|^2 + C\delta^2\sum_K \|\nabla\varphi_h\|_{L_4(K)}^4 + \frac{1}{4}\|e\|^2\\ &\quad + C\Big(\max_{S\subset\partial K} h_K^{-1}\Big)\sum_K \|h_K[\partial_s e]\|_{L_2(\partial K)} \sum_K \|[\partial_{\mathbf{n}}\varphi]\|_{L_2(\partial K)}\\ &\leqslant C\,\|\mathcal{R}\|_{L_2(\Omega)} \sum_K \|h_K[\partial_{\mathbf{n}}\varphi]\|_{L_2(\partial K)} + C|C_3|^2\sum_K \|\nabla\Theta\|_{L_2(K)}^2 + C\delta^2\sum_K \|\nabla\varphi_h\|_{L_4(K)}^4\\ &\quad + \frac{1}{2}\|e\|^2 + C\Big(\max_{S\subset\partial K} h_K^{-1}\Big)\sum_K \|[\partial_s q_h]\|_{L_2(\partial K)} \sum_K \|h_K[\partial_{\mathbf{n}}\varphi]\|_{L_2(\partial K)}.\end{aligned}$$

Letting $\psi = e$ we have proved the following *a posteriori* error estimate.

Theorem 6.2. *Let φ be the solution of the dual problem (6.1), q the solution of (4.3) and q_h the FEM-approximated solution of (4.4). Then there is a constant independent of Ω and h such that the following a posteriori error estimate holds:*

$$\|e\|^2 \leqslant Ch\Big[\big(\|\mathcal{R}_1\|_{L_2(\Omega)} + \|\mathcal{R}_2\|_{L_2(\Omega)}\big)\|\tilde{\sigma}\|_{L_2(\Omega)} + h^{-1}\big(|C_3|^2\|\mathcal{R}_3\|^2_{L_2(\Omega)} + \delta^2\|\mathcal{R}_4\|^4_{L_4(\Omega)}\big)\Big], \tag{6.20}$$

where $h = \max_K(h_K)$, $\mathcal{R}_1 = \tilde{\mathcal{R}}_1(q_h) = \Delta_h q_h + C_1\nabla q_h - \varepsilon q_h - \delta\Lambda q_h - C_2 k\sum_{i=1}^{n-1}\nabla q_{h,i}, \mathcal{R}_2 = \tilde{\mathcal{R}}_2$ is given in (6.18), $\tilde{\sigma} = [\partial_{\mathbf{n}}\varphi_h]$ and

$$\mathcal{R}_3|_K := |\nabla\Theta||_K = \nabla|V_n - V_{n,h}||_K \approx h_K|\mathcal{D}^2 V_n||_K, \qquad \mathcal{R}_4|_K := |\nabla\varphi_h||_K \approx h_K|\mathcal{D}^2\varphi||_K. \tag{6.21}$$

Note that using (3.9) and (4.14), we can estimate R_3 in (6.21) as $\mathcal{R}_3 = \nabla|V_n - V_{n,h}| \leqslant 2\xi \sim k \sim h$.

Alternatively, choosing ψ differently, we may formulate *a posteriori* error estimates as

Theorem 6.3. *Let conditions of theorem 6.2 hold and $\psi - \delta|\nabla\varphi_h|^2 = e$. Then it follows from this theorem that*

$$\|e\|^2 \leqslant Ch[(\|\mathcal{R}_1\|_{L_2(\Omega)} + \|\mathcal{R}_2\|_{L_2(\Omega)})\|\tilde{\sigma}\|_{L_2(\Omega)} + h|C_3|^2], \tag{6.22}$$

where the residual R_3 can be estimated as $\|\mathcal{R}_3\|^2_{L_2(\Omega)} \approx C_\Omega\xi^2 \sim Ch^2$, see theorem 6.2. Whereas choosing $\psi := e + \delta|\nabla\varphi_h|^2 + C_3|\nabla\Theta|$ we get the following a posteriori error estimate

$$\|e\|^2 \leqslant Ch(\|\mathcal{R}_1\|_{L_2(\Omega)} + \|\mathcal{R}_2\|_{L_2(\Omega)})\|\tilde{\sigma}\|_{L_2(\Omega)}. \tag{6.23}$$

6.1. Mesh refinement recommendation

Assume that conditions of theorem 6.3 hold. From this theorem it follows that the computational mesh should be refined in such a subdomain of the computational domain G where the computed values of the residuals $||R_1||_{L_2} + ||R_2||_{L_2}$ are maximal. Since these values are then used for the computation of the coefficient function $c(x)$, in numerical examples we take maximal values of the computed coefficient as the criterion for the refinement of the mesh.

7. The adaptive globally convergent algorithm

In this section we present our adaptive globally convergent algorithm using the mesh refinement recommendation of section 6. To this approach, on each mesh we should find an approximate solution q_n of equation (3.5). We get q_n as $q_n = \lim_{k\to\infty} q_n^k$, where k is the number of iterations with respect to the tail function $V_n(x, \bar{s})$; then, we use this function to reconstruct the coefficient $c(x)$ using the globally convergent algorithm, see [1, 2] for full details of this algorithm.

Now, for each new mesh we first linearly interpolate the function $\bar{\psi}_n$ on it, as is given in (3.3), for every pseudo-frequency interval $[s_n, s_{n-1})$. This would enable us to solve the equation for the function q_n on a new, refined mesh. Next, on every mesh we compute approximations c_n of the function $c(x)$ using the variational formulation of equation (2.6). More specifically, equation (2.6) in the domain of interest $G \setminus \Omega$ can be written as

$$\Delta w_n = (s_n)^2 c_n(x)\, w_n, \qquad \forall s_n \geqslant \underline{s} > 0. \tag{7.1}$$

Finally, we use the finite-element discretization of this equation in order to get the function c_n, noting that the function w_n is explicitly determined by $w_n = e^{V_n}$, where V_n is computed by knowing the function q_n from (2.9) and (2.12). Thus, by backward computations we can explicitly compute the coefficient function c_n on every frequency interval (s_n, s_{n-1}) through the finite-element formulation for (7.1). Note that to compute c_n we use the assumption that $c(x) = 1$ at the boundary of $G \setminus \Omega$.

As outlined in [2, 3], in the globally convergent algorithm we iterate with respect to the nonlinear term and tails. Let us denote approximations of functions c_n obtained in the globally convergent algorithm by c_n^k, where n denotes the number of the pseudo-frequency interval and k is the number of the iterations with respect to the tails. In this work we use the stopping criterion for computations for c_n^k as that of [14]. More precisely, we observe that the lower boundary Γ of the square Ω is the most sensitive boundary to the presence of inclusions. We derive this conclusion from numerical observations. Using figure 2 from the forward problem solution we observe that the low boundary of the computational domain has more reflections and thus more sensitive than other boundaries of the computational domain. This is because our maximal contrast of the function was located closer to the low boundary than to other boundaries of the computational domain.

So, if $\Gamma_{\widetilde{h}} = \left\{(x_1, x_2) \in \Omega : x_2 = -3 + \widetilde{h}\right\}$, where $\widetilde{h}$ is the mesh size in $G \setminus \Omega$, then calculating iterations with respect to the nonlinear term (see section 2 in [2]), we consider norms F_n^k, namely

$$F_n^k = ||q_n^k|_{\Gamma_{\widetilde{h}}} - \overline{\psi}_n||_{L_2(-3,3)}.$$

We stop the iterations with respect to the nonlinear term when

$$\text{either } F_n^k \geqslant F_n^{k-1} \text{ or } F_n^k \leqslant \eta, \tag{7.2}$$

where $\eta = 0.001$ is a chosen tolerance. In other words, we stop iterations, when either norms F_n^k start to grow or are too small. Next, we iterate with respect to tails and use yet another stopping criterion for computations of functions c_n^k, and once again as in the procedure in [14], we stop computing functions c_n^k when

$$\text{either } N_n \geqslant N_{n-1} \text{ or } N_n \leqslant \eta, \tag{7.3}$$

where

$$N_n = \frac{||c_n^k - c_n^{k-1}||_{L_2(\Omega)}}{||c_n^{k-1}||_{L_2(\Omega)}}. \tag{7.4}$$

We shall denote the stopping number k (on which these iterations are stopped) by m_n.

7.1. A globally convergent algorithm

Below we briefly describe a globally convergent algorithm of [1–3] which we frequently use in our computations below and in the adaptive globally convergent algorithm.

Step 0. $n_1, n \geqslant 1$. First, iterate with respect to the nonlinear term. Suppose that the functions $q_1, \ldots, q_{n-1}, q_{n,1}^0 (:= q_{n-1}) \in C^{2+\alpha}(\overline{\Omega})$ and the tail function $V_{n,0}(x, \overline{s}) \in C^{2+\alpha}(\overline{\Omega})$ are already constructed. Then, we solve iteratively the following Dirichlet boundary value problems for $k = 1, 2, \ldots$:

$$\Delta q_{n,1}^k - A_{1n}\left(h\sum_{j=1}^{n-1}\nabla q_j\right)\cdot\nabla q_{n,1}^k - \varepsilon q_{n,1}^k + A_{1n}\nabla q_{n,1}^k\cdot\nabla V_{n,0}$$
$$= 2\frac{I_{1n}}{I_0}\left(\nabla q_{n,1}^{k-1}\right)^2 - A_{2n}h^2\left(\sum_{j=1}^{n-1}\nabla q_j(x)\right)^2$$
$$+2A_{2n}\nabla V_{n,0}\cdot\left(h\sum_{j=1}^{n-1}\nabla q_j(x)\right) - A_{2n}\left(\nabla V_{n,0}\right)^2,$$
$$q_{n,1}^k = \overline{\psi}_n(x), \qquad x\in\partial\Omega.$$

As a result, we obtain the function $q_{n,1} := \lim_{k\to\infty} q_{n,1}^k$ in the $C^{2+\alpha}(\overline{\Omega})$.

Step 1. Compute $c_{n,1}$ via backward calculations using the finite-element formulation of equation (7.2).

Step 2. Solve the hyperbolic forward problem with $c_n(x) := c_{n,1}(x)$; calculate the Laplace transform and the function $w_{n,1}(x,\overline{s})$.

Step 3. Find a new approximation for the tail function

$$V_{n,1}(x) = \frac{\ln w_{n,1}(x,\overline{s})}{\overline{s}^2}. \tag{7.5}$$

Step 4. n_i, $i\geqslant 2$, $n\geqslant 1$. We now iterate with respect to the tails (7.5). Suppose that functions $q_{n,i-1}$, $V_{n,i-1}(x,\overline{s})\in C^{2+\alpha}\left(\overline{\Omega}\right)$ are already constructed.

Step 5. Solve the boundary value problem

$$\Delta q_{n,i} - A_{1n}\left(h\sum_{j=1}^{n-1}\nabla q_j\right)\cdot\nabla q_{n,i} - \kappa q_{n,i} + A_{1n}\nabla q_{n,i}\cdot\nabla V_{n,i-1}$$
$$= 2\frac{I_{1n}}{I_0}\left(\nabla q_{n,i-1}\right)^2 - A_{2n}h^2\left(\sum_{j=1}^{n-1}\nabla q_j(x)\right)^2$$
$$+2A_{2n}\nabla V_{n,i-1}\cdot\left(h\sum_{j=1}^{n-1}\nabla q_j(x)\right) - A_{2n}\left(\nabla V_{n,i-1}\right)^2,$$
$$q_{n,i}(x) = \overline{\psi}_n(x), \qquad x\in\partial\Omega.$$

Step 6. Compute $c_{n,i}$ by backward calculations using the finite-element formulation of equation (7.2).

Step 7. Solve the hyperbolic forward problem (2.1)–(2.2) with $c_n(x) := c_{n,i}$, compute the Laplace transform and obtain the function $w_{n,1}(x,\overline{s})$.

Step 8. Find a new approximation for the tail function

$$V_{n,i}(x) = \frac{\ln w_{n,i}(x,\overline{s})}{\overline{s}^2}.$$

Step 9. Iterate with respect to i until a convergence criterion as (7.4) is satisfied at $i := m_n$.

Table 1. Computational results for the globally convergent algorithm.

Iter., n	c_{n,m_n}	N_n
1	1.26	0.032 4175
2	1.33	0.033 511
3	1.4	0.036 0971
4	1.48	0.050 9878
5	1.7	0.118 18
6	1.9	0.179 527
7	3.2	0.14
8	3.8	0.16
9	3.9	0.16

Step 10. Set

$$q_n := q_{n,m_n}, \qquad c_n(x) := c_{n,m_n}(x), \qquad V_{n+1,0}(x) := \frac{\ln w_{n,m_n}(x,\bar{s})}{\bar{s}^2}.$$

Step 11. Proceed with q_{n+1} until a stopping rule (7.3) is reached.

7.2. *Adaptive globally convergent algorithm*

We use the following adaptive globally convergent algorithm in our computations.

Step 0. Choose an initial mesh K_h in Ω and an initial time partition J_0 of the time interval $(0, T)$. Compute an initial approximation c^0_{n,m_n} using the globally convergent algorithm described above on the initial mesh, see [1, 2] for details. Compute the sequence of c^j_{n,m_m}, where $j > 0$ is the number of mesh refinements, on adaptively refined meshes via the following steps.

Step 1. Compute the initial approximation for the tail function $V_n(x, \bar{s})$ on a new mesh K_h in the homogeneous medium or take initial tail as zero.

Step 2. Compute the finite-element solution $q^j_n(x, s)$ of equation (3.5) on the refined mesh K_h on the pseudo-frequency interval (s_n, s_{n-1}). Note that on this step we iterate with respect to the nonlinear term and with respect to the tails as in the globally convergent algorithm on the initial mesh above. Stopping rules for iterations with respect to the nonlinear term and tails are given in (7.2) and (7.3).

Step 3. Update the coefficient c^j_n on K_h using the finite-element formulation for (7.2).
Step 4. Stop computing c^j_n and obtain the function c^j_{n,m_n}, using the criterion (7.4).

Step 5. Refine the mesh at all the points where

$$C_h(x) \geqslant \beta_1 \max_{\Omega} c^j_{n,m_n}. \tag{7.6}$$

Here, the tolerance number $\beta_1 \in (0, 1)$ is chosen by the user, see section 8.

Step 6. Construct a new, refined mesh K_h in Ω and a new time partition J_τ of the time interval $(0, T)$ for computations of the forward problem. On J_τ the new time step τ should be chosen in such a way that the CFL condition is satisfied. Next, return to step 1 and perform all of the above steps on the new mesh.

Step 7. Stop mesh refinements if norms defined in step 4 either increase or stabilize, compared with the previous mesh, see table 1 in section 8 for the details.

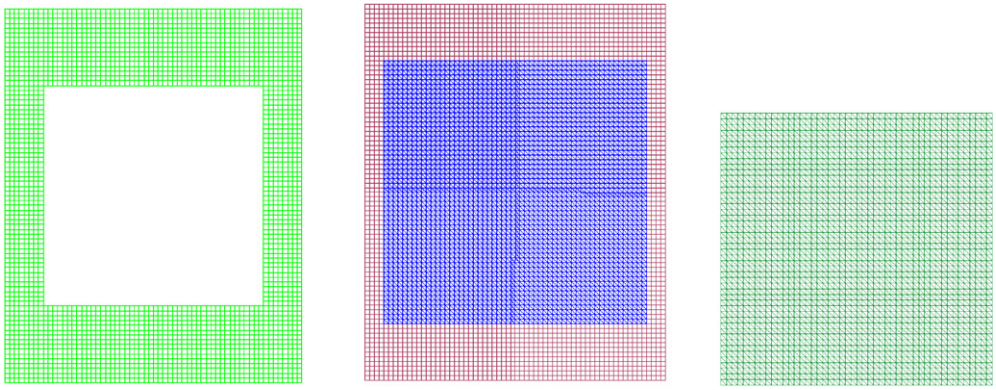

Figure 1. The hybrid mesh (b) is a combinations of a structured mesh (a), where FDM is applied, and a mesh (c), where we use FEM, with a thin overlapping of structured elements. The solution of the inverse problem is computed in the square Ω and $c(x) = 1$ for $x \in G \setminus \Omega$. (a) G_{FDM}, (b) $G = G_{\text{FEM}} \cup G_{\text{FDM}}$, (c) $G_{\text{FEM}} = \Omega$.

8. Numerical studies

8.1. Computations of the forward problem

We are working with the computationally simulated data generated by computing the forward problem with the given $c(x)$. To solve the forward problem, we use the hybrid FEM/FDM method described in [4]. The computational domain for the forward problem in our test is the domain $G = [-4.0, 4.0] \times [-5.0, 5.0]$. This domain is split into a finite-element subdomain $G_{\text{FEM}} := \Omega = [-3.0, 3.0] \times [-3.0, 3.0]$ and a surrounding region G_{FDM} with a structured mesh, $G = G_{\text{FEM}} \cup G_{\text{FDM}}$, see figure 1. We motivate our choice of using the hybrid method by the following two reasons: (i) since we know that

$$c(x) = 1, \qquad \text{in } G \setminus \Omega, \tag{8.1}$$

therefore there is no need to have a locally refined mesh in $G \setminus \Omega$, and (ii) since the inhomogeneities are located inside Ω, it is natural to use a locally fine mesh in Ω, provided by finite elements. The spatial mesh in Ω consists of triangles and in G_{FDM} of squares with the, compatible, mesh size $\widetilde{h} = 0.125$ in the overlapping regions. The boundary of the domain G is $\partial G = \partial G_1 \cup \partial G_2 \cup \partial G_3$. Here, ∂G_1 and ∂G_2 are respectively the top and the bottom sides of the largest domain in figure 1 and ∂G_3 is the union of left and right sides of this domain. At ∂G_1 and ∂G_2 we use first-order absorbing boundary conditions, namely [10]. The trace of the solution of the forward problem is recorded at the boundary $\partial\Omega$. Next, the coefficient $c(x)$ is 'forgotten', and our goal is to reconstruct this coefficient for $x \in \Omega$ from the data $g(x, t)$, see (2.4).

Thus, the forward problem in our test is

$$\begin{aligned}
&c(x)u_{tt} - \triangle u = 0, && \text{in} \quad G \times (0,T),\\
&u(x,0) = 0, && \text{in} \quad G,\\
&u_t(x,0) = 0, && \text{in} \quad G,\\
&u(x,t) = f(t), && \text{on} \quad \partial G_1 \times (0,t_1],\\
&\partial_n u(x,t) = -\partial_t u(x,t), && \text{on} \quad \partial G_1 \times (t_1,T),\\
&\partial_n u(x,t) = -\partial_t u(x,t), && \text{on} \quad \partial G_2 \times (0,T),\\
&\partial_n u(x,t) = 0, && \text{on} \quad \partial G_3 \times (0,T),
\end{aligned} \tag{8.2}$$

where $f(t)$ is the plane wave defined as

$$f(t) = \frac{(\sin(\bar{s}t - \pi/2) + 1)}{10}, \qquad 0 \leqslant t \leqslant t_1 := \frac{2\pi}{\bar{s}}, \qquad T = 17.8\, t_1.$$

Thus, the plane wave is initialized at the top boundary ∂G_1 and propagates into G for $t \in (0, t_1]$. First-order absorbing boundary conditions [10] are used on top $\partial G_1 \times (t_1, T]$ and bottom $\partial G_2 \times (0, T]$ boundaries, and the Neumann or mirror boundary condition is used on $\partial G_3 \times (0, T]$. Figure 2 shows how the plane wave propagates for the structure given in figure 4(a).

We compare our computational solution of the forward problem (8.2) obtained by using finite element, finite difference and hybrid methods, with the analytical solution. We use different meshes in order to select an optimal mesh size h in the computations. We define the plane wave in (8.2) as

$$f(t) = \begin{cases} \sin(\omega t), & \text{if} \quad t \in \left(0, \dfrac{2\pi}{\omega}\right), \\ 0, & \text{if} \quad t > \frac{2\pi}{\omega}. \end{cases} \tag{8.3}$$

The analytical solution of the problem (8.2) with $c = 1$ is given by the following formula, see [7]:

$$u(y,t) = \begin{cases} 0, & \text{if} \quad t \in (0, a - y) \\ \sin\omega(t - a + y), & \text{if} \quad t \in \left(a - y, a - y + \dfrac{2\pi}{\omega}\right), \\ 0, & \text{if} \quad t > a - y + \frac{2\pi}{\omega}, \end{cases} \tag{8.4}$$

where y is the vertical coordinate and we consider equation (8.2) in the domain $R_a = \{y < a\}, a = \text{const.} \geqslant 0$. In order to perform computations of the forward problem in an optimal way, we need to choose *optimal*, computational parameters such as the mesh size h and the time step τ. We compute the forward problem at every iteration in the globally convergent algorithm (we shall need it for computing of the tail function $V(x, \bar{s})$, see algorithms in section 7). Thus, we want to reduce the computational time when computing the solution for the problem (8.2) without losing the important information from this solution when solving the inverse problem. Figure 3 presents comparison between the exact solution given by (8.4) and the computed solutions for the problem (8.2), at different points of the computational domain G when computing with different mesh sizes. We observe that exact and computed solutions have main difference at the bottom of the computational domain G. The computed solution on the mesh with the mesh size $h = 0.05$ approximates the exact solution more accurately, and the computed solution with the mesh size $h = 0.1$ has twice smaller amplitude after the time iteration. We tested the solution of our inverse problem on different meshes and it turns out that the mesh size $h = 0.05$ gives a similar solution for the inverse problem as computations on the meshes with mesh sizes $h = 0.1$ and $h = 0.125$. On the other hand, compared with

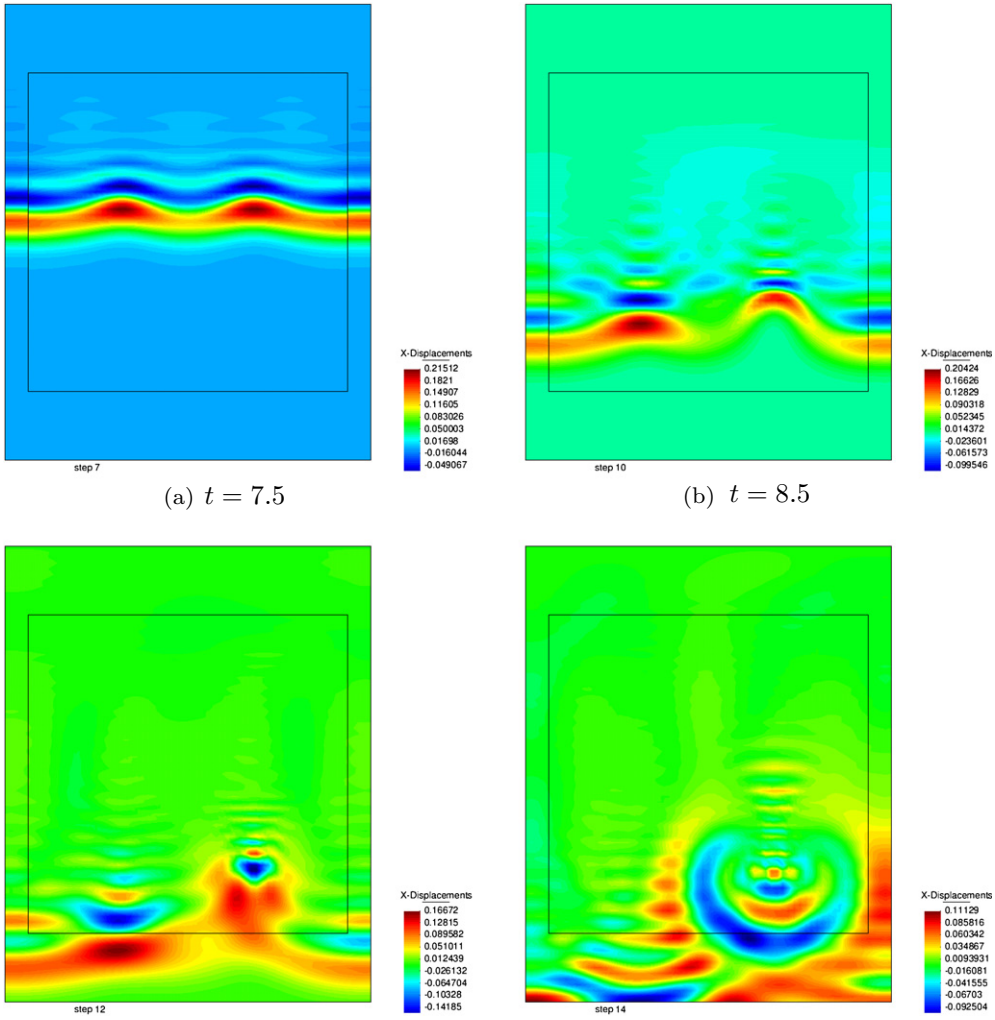

(a) $t = 7.5$ (b) $t = 8.5$

(c) $t = 9.6$ (d) $t = 11.2$

Figure 2. Isosurfaces of the simulated exact solution to the forward problem (8.2) at different times with a plane wave initialized at the top boundary.

the computations on the mesh with $h = 0.125$, computations on the mesh size $h = 0.05$ are very much time consuming. Therefore, in computations below we use computations of the forward problem on the mesh size $h = 0.125$.

8.2. Reconstruction by the globally convergent algorithm

In this numerical experiment we reconstruct the medium, where $c(x)$ is defined as follows:

$$c(x) = \begin{cases} 1 + 0.5\left(\sin\left(\dfrac{\pi}{3}x\right)\right)^2 \cdot (\sin(\pi/3)y)^2, & -3 \leqslant x < 0 \quad \text{and} \quad -3 \leqslant y < 3; \\ 1 + 0.5\left(\sin\left(\dfrac{\pi}{3}x\right)\right)^2 \cdot (\sin(\pi/3)y)^2, & 0 \leqslant x \leqslant 3 \quad \text{and} \quad 0 \leqslant y \leqslant 3; \\ 1 + 3.0\left(\sin\left(\dfrac{\pi}{3}x\right)\right)^2 \cdot (\sin(\pi/3)y)^2, & 0 \leqslant x \leqslant 3 \quad \text{and} \quad -3 \leqslant y \leqslant 0; \end{cases} \tag{8.5}$$

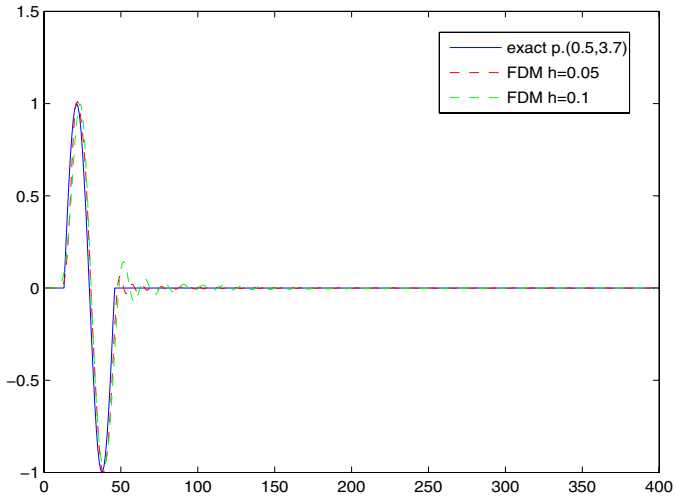

(a)

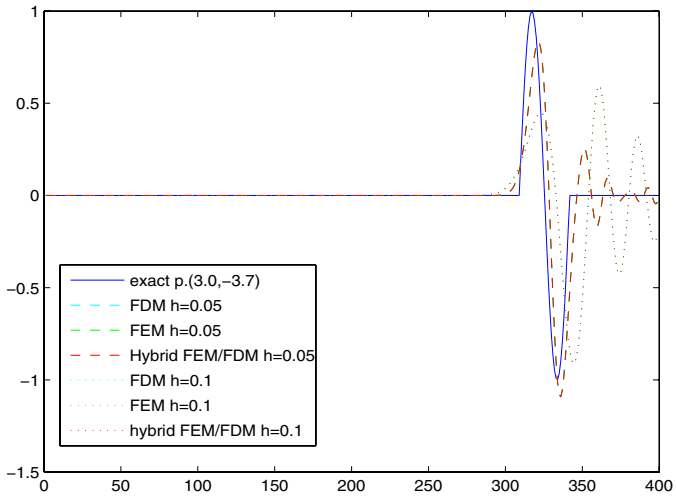

(b)

Figure 3. Exact and computed solutions of the equation using different methods: (a) comparison of exact solution and computed solutions at the point (0.5, 3.7), which is located at the top of the computational domain G; (b) comparison of the exact solution and computed solutions at the point (3.0, −3.7), which is located at the bottom of the computational domain G.

see figure 4(a). Note that we have not assumed *a priori* knowledge of neither the structure of this medium nor of the background constant $c(x) = 1$ outside of the medium Ω, but we have assumed the knowledge of the lower bound $c(x) \geqslant 1$ and also that outside of the domain of interest Ω our function $c(x) = 1$. This explains why our starting value for the tail function is $V_{1,1}(x) = \overline{s}^{-2} \ln \widetilde{w}(x, \overline{s})$, where $\widetilde{w}(x, \overline{s})$ is the function $w(x, s)$ at $s = \overline{s}$ for the case $c \equiv 1$.

It was shown (see [1, 2]) that the interval $[\underline{s}, \overline{s}] = [6.7, 7.45]$ is the optimal one for the domains G and Ω. We choose the step size with respect to the pseudo-frequency $\rho = 0.05$. In our example we let $N = 15$ and choose regularization parameters $\lambda := 20$ in the Carleman

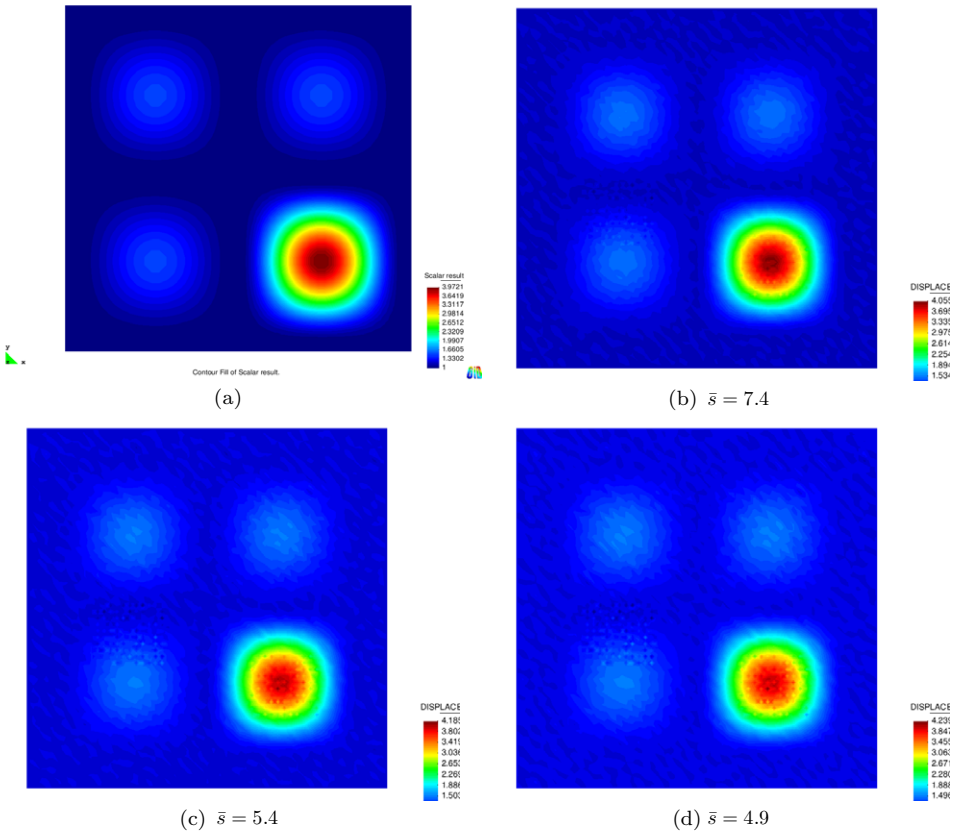

(a) (b) $\bar{s} = 7.4$ (c) $\bar{s} = 5.4$ (d) $\bar{s} = 4.9$

Figure 4. Exact (on (a)) and computed (on (b), (c), (d)) coefficients $c(x)$ using the exact computed values of the tail function $V(x, \bar{s})$.

weight function (3.4) and $\varepsilon = 0.0$ in (3.5) for $n = 1, \ldots, N$. Once the function $q_{n,k}$ is calculated, we update the function $c := c_{n,k}$ by backward calculations (see the algorithm in section 7.1). The resulting computed function is $c_{n,m_n} := c_{\overline{N}}(x)$. In our numerical test we have considered the noisy boundary data g_σ introduced by

$$g_\sigma\left(x^i, t^j\right) = g\left(x^i, t^j\right)\left[1 + \frac{\varsigma_j (g_{\max} - g_{\min})\sigma}{100}\right].$$

Here, $g\left(x^i, t^j\right) = u\left(x^i, t^j\right)$, where $x^i \in \partial\Omega$ is a mesh point at the boundary $\partial\Omega$, $t^j \in (0, T)$ is a mesh point in time, ς_j is a random number in the interval $[-1; 1]$, $g_{\max}$ and $g_{\min}$ are respectively maximal and minimal values of the computed boundary data g in (2.5) and $\sigma = 5\%$ is the noise level.

Since we have (8.1), we set $2d_1 = 1$. Instead of using the extension procedure described in the beginning of section 5 of [3], we simply set $c_{n,k}(x) := 1$ in $G \setminus \Omega$. In addition, since by (2.3) we need the *a priori* lower bound $c(x) \geqslant d_1$, we enforce that the coefficient $c(x)$ belongs to the set of admissible coefficients $C_{\text{adm}} = \{c(x) \geqslant 0.5\}$ as follows. If $c_{n,k}(x_0) < 0.5$ for a certain point $x_0 \in \Omega$ and a certain pair (n, k), then we set $c_{n,k}(x_0) := 1$. The only reason why we use the value 1 in this setting is that we are supposed to know that condition (8.1) is satisfied. Therefore, this setting as well as the fact that we allow the function $c(x)$ to attain

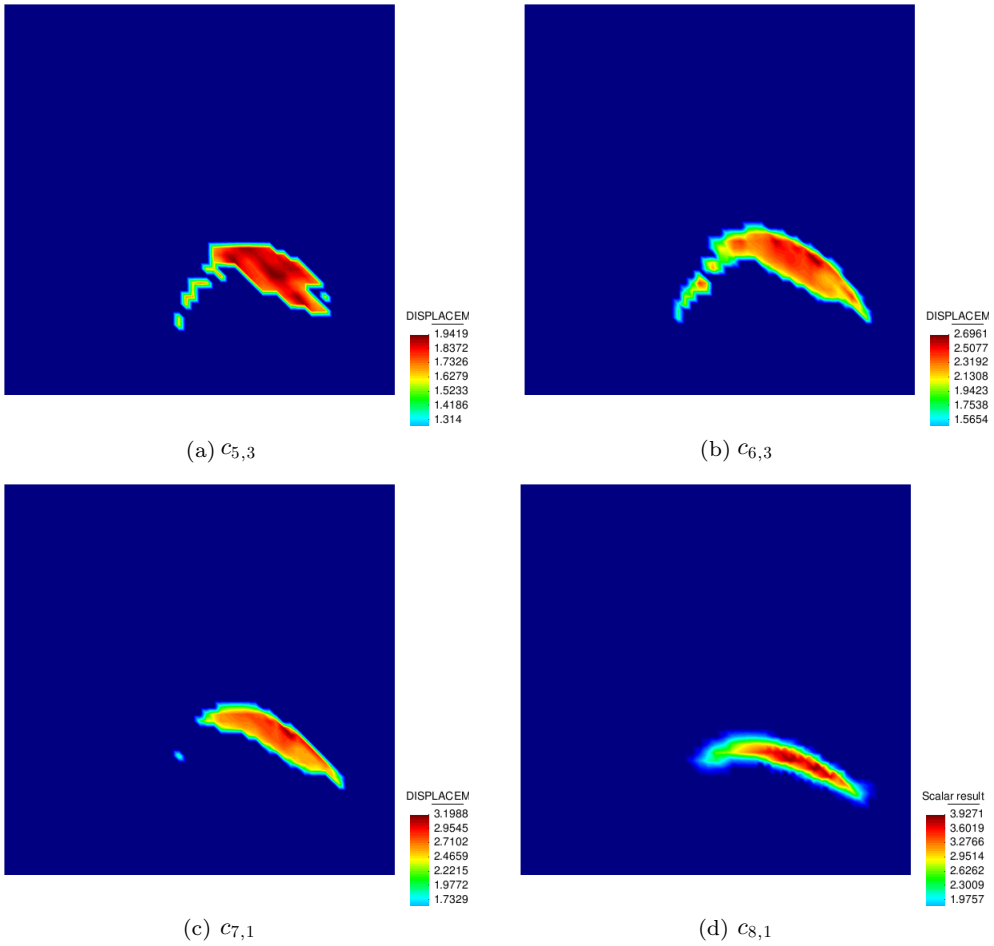

(a) $c_{5,3}$ (b) $c_{6,3}$

(c) $c_{7,1}$ (d) $c_{8,1}$

Figure 5. Results of the performance of the globally convergent algorithm of section 7.1. Spatial distributions of some functions $c_{n,k}$. The function $c_{8,1}$ is taken as the final result. The maximal value of $c_{8,1}(x) = 3.8$ within the maximal value of function (8.5). Also, $c_{8,1}(x) = 1$ outside of this maximal value. Hence, the 3.8:1 inclusion/background contrast is imaged well (the correct maximal value of function (8.5) is 4:1). However, the form of the imaged function is desirable to be improved. This is why we apply the adaptive globally convergent algorithm, which takes the function $c_{8,1}$ for the refinement criterion (7.6).

values between 0.5 and 1 does not mean that we assume the knowledge of the background value of the function $c(x)$. In principle, this constraint cannot guarantee either the continuity of the resulting function $c_{n,k}(x)$ or that $c_{n,k}(x) \geqslant 1$. Nevertheless, we have observed in our numerical tests of this publication and in [3, 4, 5] that all resulting functions $c_{n,k}$ are continuous and $c_{n,k}(x) \geqslant 1$ for all x, i.e. 'allowed' values between 0.5 and 1 are not actually attained in iterations.

Figure 5 displays results of the performance of the globally convergent algorithm. One can see that the location of the maximal value of the function (8.5) is imaged very well. It follows from figure 5(d) that the imaged contrast in this function is 3.8:1 $=$ max $c_{8,1}$:1, where $n := \overline{N} = 8$ is our final iteration number (see below for the choice of $\overline{N}$). However, the

Table 2. Set of admissible parameters in different tests.

Test 1	$c \in P = \{c \in C(\overline{\Omega}) \mid 1 \leqslant c(x) \leqslant 8\}$
Test 2	$c \in P = \{c \in C(\overline{\Omega}) \mid 1 \leqslant c(x) \leqslant 5\}$
Test 3	$c \in P = \{c \in C(\overline{\Omega}) \mid 1 \leqslant c(x) \leqslant 16\}$

values of $1 + 0.5(\sin(\frac{\pi}{3}x))^2 \cdot (\sin(\pi/3)y)^2$ in (8.5) are not reconstructed but are smoothed out. Thus, we are able to reconstruct only maximal values of the function (8.5). Comparison with figure 4(a) reveals that it is desirable to improve the shape of the function. This explains why we decided for the subsequent application of the adaptivity technique inside the globally convergent algorithm.

Using table 1, we analyze results of our reconstruction. We observe that the norms N_n in criterion (7.4) increase until computing the function q_6. Next, these norms slightly decrease and stabilize for $n = 8, 9$. For $n = 10, \ldots, 15$ the norms grow steeply; these cases are not presented in the table. Thus, we conclude that we should stop our iterations at $\overline{N} = 8$. So, we take the function $c_{8,1} := c_{\text{glob}}$ as our final reconstruction result on the globally convergent stage.

8.3. Reconstruction by the adaptive globally convergent algorithm

In this subsection, we demonstrate the performance of the adaptive globally convergent algorithm given in section 7.2. The question we discuss now is how to choose the tolerance number β_1 in (7.6). If we choose $\beta_1 \approx 0$, then we will refine the mesh in almost the entire domain Ω, since the function $c_{n,m_n} > 0$. We note that our goal is to construct a new locally refined mesh with as few nodes as possible. The parameter β_1 cannot be taken too close to 1 either, since then the automatic adaptive algorithm would come up with a too narrow region, where the mesh should be refined. Thus, the choice of β_1 depends on concrete values of the function $C_h(x)$ and should be chosen in numerical experiments. So, we take $\beta_1 = 0.6$ on the initial coarse mesh and for all follow-up refinements of the initial mesh, and refine the mesh at the all points located in the circle with the center at $\max_\Omega c^0_{n,m_n}$ and with radius $r = \beta_1 \max_\Omega c^0_{n,m_n}$.

In the adaptive algorithm we can use box constraints for the reconstructed coefficient. We obtain these constraints using the solution computed in the globally convergent method. Since the function $c_{\text{glob}} = c^0_{n,m_n}$ obtained in the globally convergent algorithm is a good approximation for the correct solution, and $c_{\text{glob}}(x) \in [1, 3.8]$, we can enforce the coefficient $c(x)$ to belong to the following set of admissible parameters $c \in P = \{c \in C(\overline{\Omega}) \mid 1 \leqslant c(x) \leqslant 5\}$. We use this set in test 2; see table 2 for other two set of admissible parameters. To check the accuracy of the adaptive globally convergent method, we decided to check three different sets of tests.

In all three tests, we start with the function $c_{\text{glob}}(x)$ on the initial coarse mesh shown in figure 5(d), use it in criterion (7.6) and refine the coarse mesh. Then we perform all steps of the adaptive globally convergent algorithm to obtain the function c^1_{n,m_n}. We analyze the results of this reconstruction by using table 3.

8.3.1. Test 1. We observe that after one refinement of the mesh the norms N_n in criterion (7.4) are first stabilized until computing the function q_4, see table 3. Next, these norms slightly

Table 3. Computational results for the adaptive globally convergent algorithm.

Test 1			Test 2			Test 3		
Iter., n	c^1_{n,m_n}	N_n	Iter., n	c^1_{n,m_n}	N_n	Iter., n	c^1_{n,m_n}	N_n
1	1.6	0.05	1	1.87	0.038	1	1.6	0.38
2	1.5	0.04	2	1.43	0.09	2	1.5	0.09
3	1.6	0.05	3	1.48	0.13	3	1.6	0.13
4	1.6	0.05	4	1.53	0.16	4	1.6	0.16
5	1.7	0.16	5	1.59	0.2	5	1.7	0.2
6	1.6	0.16				6	1.6	0.2
Iter., n	c^2_{n,m_n}	N_n	Iter., n	c^2_{n,m_n}	N_n	Iter., n	c^2_{n,m_n}	N_n
1	1.9	0.08	1	2.45	0.04	1	1.9	0.04
2	3.99	0.34	2	4.0	0.25	2	3.99	0.5
3	3.99	0.33	3	4.0	0.25	3	3.99	0.5
4	3.99	0.33	4	4.0	0.25	4	3.99	0.44
						5	3.99	0.38
			Iter., n	c^3_{n,m_n}	N_n			
			1	2.25	0.04			
			2	3.8	0.16			
			3	3.9	0.16			
			4	4.0	0.16			

increase and again stabilize on $n = 5, 6$. For $n = 7, \ldots, 10$, these norms grow steeply (which are not presented in the table). Thus, we conclude, that we should stop the iterations at $\overline{N} = 1$. So, we take the function $c^1_{1,4}$ as our final reconstruction result on the first iteration of the adaptive refinement procedure. Comparing figures 5(d) and 6(b) shows that the image has not improved significantly, compared to the one obtained on the globally convergent stage.

Next, we refine the mesh locally, again using the criterion (7.6) and the same function $c_{\text{glob}}(x)$ as shown in figure 5(d), and perform the algorithm of section 7.2. One can see in figure 6(f) that we are able to accurately reconstruct location, shape and contrast of the maximal values of the function (8.5). The value of the coefficient $c(x) = 1$ outside of the support of the function (8.5) is also imaged very well. Using table 2, we analyze again results of our reconstruction on a twice refined mesh. We observe that the norms N_n in the criterion (7.4) increase very fast until computing the function q_2. Then, these norms are stabilized on steps $n = 2, 3, 4$. For the steps $n = 5, \ldots, 7$, the norms grow steeply; we do not present these norms in the table. Hence, we conclude that one should stop the iterations at $\overline{N} = 2$. So, we take the function $c^2_{2,1}$ as our final reconstruction result on twice adaptively refined mesh.

8.3.2. Test 2. In test 2 we take the maximal value in the set of admissible parameters for c to be $c = 5$, see table 2, which is close to the globally convergent solution obtained on the coarse mesh. We observe that after one refinement of the mesh the norms N_n in the criterion (7.4) reaches a maximal value at q_1, and then they grow until computing the function q_5, see table 3. This time, for $n = 6, \ldots, 10$, the norms grow rapidly, which and are not presented in the table. Thus, we conclude that we should stop our iterations at $\overline{N} = 1$. So, we take the function $c^1_{1,1}$ as the final reconstruction result on the first adaptively refined mesh. This time the images are not improved and we have not presented them in here.

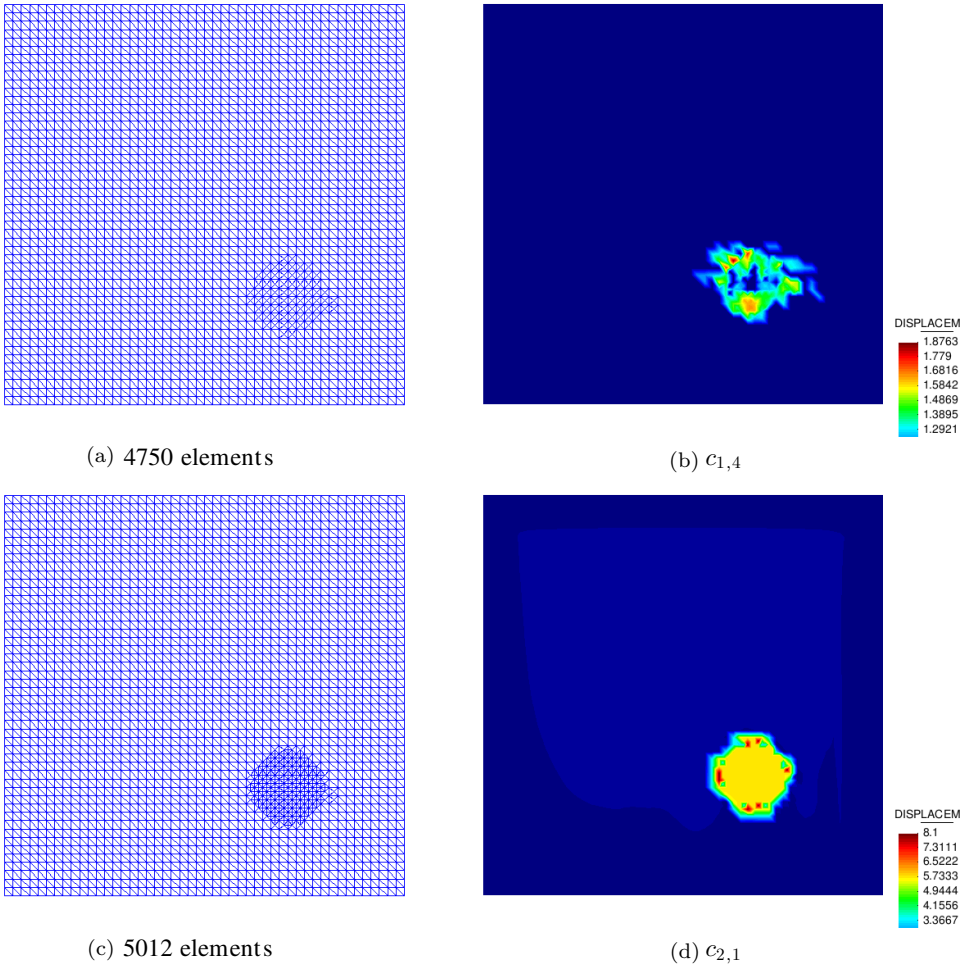

(a) 4750 elements (b) $c_{1,4}$

(c) 5012 elements (d) $c_{2,1}$

Figure 6. Test 1: adaptively refined meshes (a), (c) and corresponding images (b)–(d) using the adaptive globally convergent algorithm of section 7.2. In this test we choose the set of admissible parameters for the coefficient $c \in P = \{c \in C(\overline{\Omega}) | 1 \leqslant c(x) \leqslant 8\}$. Locations of maximum value of the function (7.6) as well as shape and 4:1 contrasts in them are imaged accurately, see the details in the text and compare with figure 6(d).

Next, we refine the mesh locally again, as in test 1, we observe in figure 7(b) that we are able to very accurately reconstruct location, shape and contrast of the maximal values of the function (8.5). We observe that the norms N_n in the criterion (7.4) increase very fast until computing the function q_2. These norms are stabilized on $n = 2, 3, 4$. For $n = 5, \ldots, 7$, the norms grow rapidly and are not presented in the table. Thus, we stop the iterations at $\overline{N} = 2$, and hence, we take the function $c^2_{2,1}$ as our final reconstruction result on the twice adaptively refined mesh. This result is similar to the results of test 1; the contrast here is better and very much closer to the exact one.

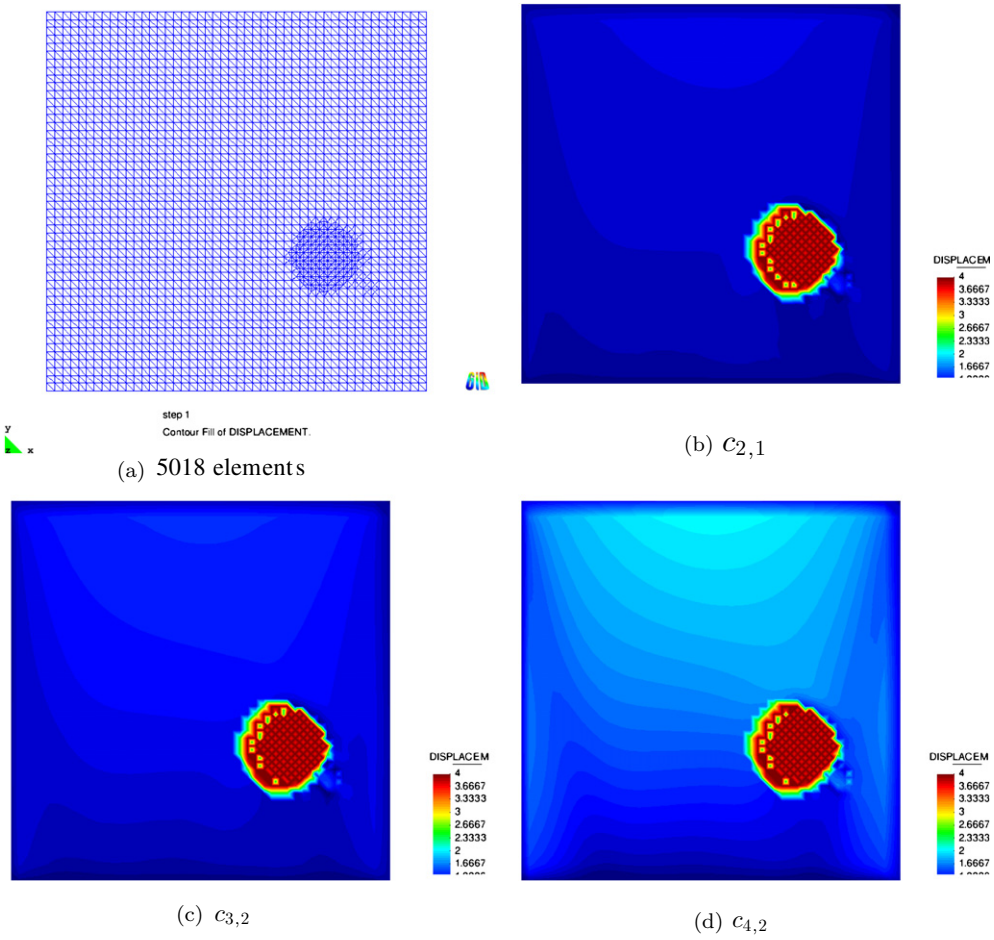

(a) 5018 elements (b) $c_{2,1}$

(c) $c_{3,2}$ (d) $c_{4,2}$

Figure 7. Test 2: adaptively refined mesh (a) and corresponding images (b)–(d), using the adaptive globally convergent algorithm of section 7.2. In this test we choose set of admissible parameters for coefficient $c \in P = \{c \in C(\overline{\Omega}) | 1 \leqslant c(x) \leqslant 5\}$. Locations of maximum value of the function (7.6) as well as shape and 4:1 contrasts in them are imaged accurately, see details in the text and compare with figure 6(d).

8.3.3. Test 3. In this last test we take the maximal value in the set of admissible parameters for c to be $c = 16$, see table 2, that is very far from the exact one. Our goal now is to check whether we get reconstruction results similar to previous ones. We observe that, after first refinement of the mesh, we get similar results as the previous tests and the images are not improved.

Next, we make a twice refinement of the mesh using the criterion (7.6). One can see in figure 8(b) that we are still able to reconstruct location, shape and contrast of the maximal values of the function (8.5), but not as accurately as in the previous tests. The value of the coefficient $c(x) = 1$ outside of the support of the function (8.5) is also imaged well. Using table 3, we analyze again results of our reconstruction on the two times refined mesh. We observe that the norms N_n in the criterion (7.4) increases very fast until computing the function

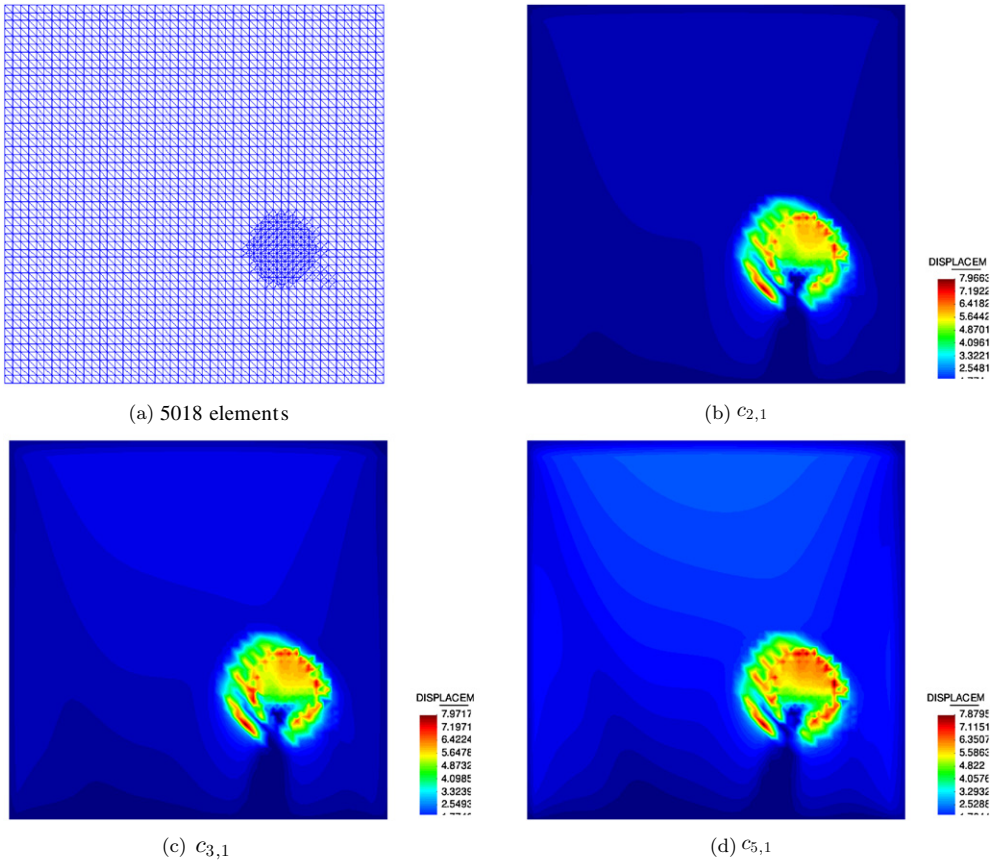

(a) 5018 elements (b) $c_{2,1}$

(c) $c_{3,1}$ (d) $c_{5,1}$

Figure 8. Test 3: adaptively refined mesh on (a) and corresponding images on (b)–(d), using the adaptive globally convergent algorithm of section 7.2. In this test we choose a set of admissible parameters for the coefficient $c \in P = \{c \in C(\overline{\Omega}) | 1 \leqslant c(x) \leqslant 16\}$. Locations of maximum value of the function (7.6) as well as shape and main contrast 4:1 in them are imaged accurately, see the details in the text and compare with figure 5(d).

q_2 and then they have a similar behavior as in previous tests. So, we take the function $c^2_{2,1}$ as our final reconstruction result on the two times adaptively refined mesh.

8.4. Conclusion of numerical experiments

Summing up, we can conclude that the location, shape and maximal contrast of the reconstructed function compared to the background medium can be reconstructed accurately using the new adaptive globally convergent algorithm. Our numerical experiments show that the contrast of the reconstructed function and that of the exact one would be the same if we take the maximal value in the set of admissible parameters close to the exact one, and almost the same as in the exact function if we take maximal value in the set of admissible parameters far from the exact one. This shows the flexibility of our adaptive algorithm and can be used, for example, in the globally convergent algorithm using convexification algorithms, when locations of inclusions are well reconstructed, but contrast needs to be improved [16].

We also note that we tested a two-stage numerical procedure developed in [2, 3] on reconstruction of the function (8.5) and we get similar results of reconstruction as thus obtained in section 8.3, see figures 6–8. Thus, we have a very good agreement between the exact data and the numerical experiments. Our future work will be concentrated on the application of the adaptive globally convergent numerical method for *the accurate reconstruction of the shape and the contrast of the inclusions*.

Acknowledgments

The research of the authors was partially supported by the Swedish Foundation for Strategic Research (SSF) in the Gothenburg Mathematical Modelling Centre (GMMC) and by the Swedish Institute, Visby Program. The authors are grateful to Professor M V Klibanov and to an anonymous referee for his useful comments which helped improve the presentation.

References

[1] Beilina L and Klibanov M V 2008 A globally convergent numerical method for a coefficient inverse problem *SIAM J. Sci. Comp.* **31** 478–509
[2] Beilina L and Klibanov M V 2010 *A posteriori* error estimates for the adaptivity technique for the Tikhonov functional and global convergence for a coefficient inverse problem *Inverse Problems* **26** 045012
[3] Beilina L and Klibanov M V 2010 Synthesis of global convergence and adaptivity for a hyperbolic coefficient inverse problem in 3D *J. Inverse and Ill-posed Problems* **18** 85–132
[4] Beilina L, Samuelsson K and Åhlander K 2001 Efficiency of a hybrid method for the wave equation *Int. Conf. Finite Element Methods (Gakuto International Series: Mathematical Sciences and Applications)* (Gakkotosho)
[5] Belishev M I 1997 Boundary control in reconstruction of manifolds and metrics (the BC method) *Inverse Problems* **13** R1–45
[6] Belishev M I and Gotlib V Yu 1999 Dynamical variant of the BC-method: theory and numerical testing *Inverse Ill-Posed Problems* **7** 221–40
[7] Budak B M, Samarskii A A and Tikhonov A N 1988 *A Collection of Problems in Mathematical Physics* (New York: Dover)
[8] Burov V A, Morozov S A and Rumyantseva O D 2002 Reconstruction of ne-scale structure of acoustical scatterers on large-scale contrast background *Acoustical Imaging* **26** 231–8
[9] Cheney M and Isaacson D 1995 Inverse problems for a perturbed dissipative half-space *Inverse Problems* **11** 865–88
[10] Engquist B and Majda A 1977 Absorbing boundary conditions for the numerical simulation of waves *Math. Comp.* **31** 629–51
[11] Johnson C and Szepessy A 1995 Adaptive finite element methods for conservation laws based on *a posteriori* error estimation *Comm. Pure Appl. Math.* **48** 199–234
[12] Klibanov M V and Timonov A 2004 *Carleman Estimates for Coefficient Inverse Problems and Numerical Applications* (Utrecht, The Netherlands: VSP)
[13] Klibanov M V 1991 Inverse problems and Carleman estimates *Inverse Problems* **8** 575–96
[14] Klibanov M V, Fiddy M A, Beilina L, Pantong N and Schenk J 2010 Picosecond scale experimental verification of a globally convergent numerical method for a coefficient inverse problem *Inverse problems* **26** 045003
[15] Klibanov M and Timonov A A 2004 A unified framework for constructing of globally convergent numerical algorithms for multidimensional coefficient inverse problems *Appl. Anal.* **83** 933–55
[16] Kuzhuget A V and Klibanov M V 2010 Global convergence for a 1-d inverse problem with application to imaging of land mines *Appl. Anal.* **89** 1, 125–57
[17] Mueller J and Siltanen S 2003 Direct reconstructions of conductivities from boundary measurements *SIAM J. Sci. Comp.* **24** 1232–66
[18] Nachman A 1996 Global uniqueness for a two-dimensional inverse boundary value problem *Ann. Math.* **143** 71–96

[19] Novikov R G 1988 Multidimensional inverse spectral problem for the equation .. + (v(x) .. eu(x)) = 0 *Funct. Anal. Appl.* **22** 11–22
[20] Novikov R G 2005 The $\overline{\partial}$ approach to approximate inverse scattering at fixed energy in three dimensions *Int. Math. Res. Papers* **6** 287–349
[21] Tikhonov A N and Arsenin V Y 1977 *Solutions of Ill-Posed Problems* (Washington, DC: Winston)